Coordination Chemistry Reviews 513 (2024) 215866

Contents lists available at ScienceDirect

Coordination Chemistry Reviews

journal homepage: www.elsevier.com/locate/ccr

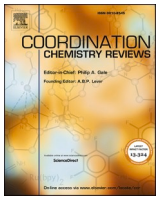

Review

Organic dye-based photosensitizers for fluorescence imaging-guided cancer phototheranostics

Rui Wang [a,b], Siwei Hua [b], Yanlong Xing [a,b], Rui Wang [a,b], Huimin Wang [a], Tongmeng Jiang [a,b,*], Fabiao Yu [a,b,*]

[a] Key Laboratory of Hainan Trauma and Disaster Rescue, Key Laboratory of Haikou Trauma, The First Affiliated Hospital of Hainan Medical University, Hainan Medical University, Haikou 571199, China
[b] Engineering Research Center for Hainan Bio-Smart Materials and Bio-Medical Devices, Key Laboratory of Emergency and Trauma, Ministry of Education, Key Laboratory of Hainan Functional Materials and Molecular Imaging, College of Emergency and Trauma, Hainan Medical University, Haikou 571199, China

ARTICLE INFO

Keywords:
Fluorescence imaging-guided photo-theranostics
Cancer treatment
Photosensitizers
Monomers
Nanoparticals

ABSTRACT

Precise diagnosis and treatment of tumors is the current hotspot, which has also given rise to a new subject named "theranostics". It is an ideal precision treatment strategy if the agent can provide effective treatment while visually monitoring tumor occurrence and providing timely feedback on the efficacy. Fluorescence imaging-guided phototherapy technology is a non-invasive, simple-to-operate, highly safe and non-drug-resistant visual treatment method that can accurately monitor tumor sites, perform efficient phototherapy and feedback on tumor treatment effects. Photosensitizers with fluorescence imaging capabilities play a decisive role in the entire diagnosis and treatment process. In this review, we focus on four commonly used photosensitizers with fluorescence imaging functions, including cyanine, tetrapyrrole structures, BODIPY, and AIEgens. The design strategies and principles for improving imaging or/and therapeutic functions were highlighted based on these four organic molecular monomers or their nanoaggregates, nanocomposites, etc. The challenges and future opportunities of fluorescence imaging-guided phototherapy in the clinical translation of precision tumor treatment are also presented.

1. Introduction

Tumors have the characteristics of high incidence rate, strong concealment in the early stage, complexity and heterogeneity of the occurrence and development process, as well as easy recurrence and metastasis, making them a killer that seriously reduces the quality of life and endangers life and health [1–3]. Traditional single or combined treatment methods such as surgery, chemotherapy, and radiotherapy are still the conventional means of clinical treatment of tumors [4,5]. Frustratingly, the above-mentioned treatments still face shortcomings such as high invasiveness, low targeting, and high side effects [6,7]. They are also unable to achieve real-time visual diagnosis of tumors and timely feedback on therapeutic effects. Therefore, the development of new imaging-guided, non-invasive and low-side-effect theranostic methods is of great significance for the precise treatment of tumors [8–10].

The non-invasive, highly selective, and low-drug-resistant phototherapy has attracted widespread attention from medical workers and scientific researchers since it was used in the clinical treatment of various types of tumors more than 40 years ago [4,11]. Photodynamic therapy (PDT) and photothermal therapy (PTT) are important components of phototherapy, which can selectively treat diseased areas and have great therapeutic effects on various types of tumors [12]. Not only that, phototherapy does not conflict with other treatments, and each treatment takes less time, making life more convenient [13,14].

Light, photosensitizers (PSs), oxygen (or other adjacent substrates) are indispensable and vital components of PDT [15,16]. After the PS in the ground state (S_0) absorbs excitation light of a specific wavelength, it produces toxic reactive oxygen species (ROS), damaging prominent proteins and subcellular organelles, thereby inducing apoptosis of tumor cells [17,18]. PDT is used for anti-tumor treatment in three interrelated ways: (1) directly killing tumor cells; (2) damaging tumor blood vessels; (3) activating the immune system [19]. Different from PDT, the PS absorbs laser of a specific wavelength and reaches to the excited state from

* Corresponding authors at: Key Laboratory of Hainan Trauma and Disaster Rescue, Key Laboratory of Haikou Trauma, The First Affiliated Hospital of Hainan Medical University, Hainan Medical University, Haikou 571199, China.
E-mail addresses: ruiwang@hainmc.edu.cn (R. Wang), jiangtongmeng@hainmc.edu.cn (T. Jiang), yufabiao@hainmc.edu.cn (F. Yu).

https://doi.org/10.1016/j.ccr.2024.215866
Received 2 January 2024; Received in revised form 6 March 2024; Accepted 5 April 2024
Available online 2 May 2024
0010-8545/© 2024 Elsevier B.V. All rights reserved.

the S_0, and then returns to the S_0 through non-vibrational relaxation is called PTT process [20]. At the same time, it releases enough heat to damage the membrane structure of tumor cells or cause the inactivation of proteins and other substances, thereby achieving the purpose of tumor elimination [21,22].

Since phototherapy has inherent selectivity for disease treatment, it only needs to give light to the lesion, thereby reducing damage to normal tissue and reducing side effects [4,23]. Based on this, the best treatment timing can be determined by real-time monitoring of the distribution of PSs in the body and its enrichment time at the tumor site, so as to achieve the lowest drug dose and the best therapeutic effect. Fluorescence imaging technology is a high-profile non-invasive imaging method with great sensitivity and resolution [24–27]. By combining fluorescence imaging technology and phototherapy, the targeting effect, therapeutic efficiency and metabolic effect of PSs on tumor sites can be determined, thereby clarifying the entire dynamic process of PSs in the body and laying a theoretical foundation for clinical translation [28]. As an essential part of fluorescence imaging, fluorophores can emit fluorescence by absorbing light of specific wavelengths [29]. Fortunately, many fluorophores have been structurally modified to possess phototherapeutic properties [30]. Therefore, the development of these PSs with fluorescence imaging properties provides a feasible strategy for real-time diagnosis and precise treatment of tumors [31,32].

The performance of phototheranostic agents directly determines the effects of fluorescence imaging and phototherapy. Hundreds of PSs, including porphyrins, phthalocyanines, boron dipyrromethene (BODIPY), etc., have been used in clinical research on various solid tumors [33–35]. An ideal PS should have the following properties [33,36,37]: (1) High operability, many sites that can be modified, and simple structural modification; (2) It can possess excellent tumor targeting by itself or after modification; (3) The absorption mainly in the near-infrared region (NIR, 700–1350 nm; NIR I and NIR II), which is beneficial to reducing the interference of biological autofluorescence background and decreasing the inconvenience of life caused by the strictly avoiding light after treatment; (4) Superior quantum yield of ROS for PDT and excellent photothermal conversion efficiency (PCE) for PTT; (5) Strong safety, no dark toxicity, high biocompatibility, and easily metabolized out of the body. To meet the above requirements, researchers have designed and synthesized a series of organic molecules with fluorescent diagnostic and therapeutic functions, or constructed nanoaggregates, nanocomposites, and nanomaterials based on these functional molecules through self-assembly or co-assembly for fluorescence imaging-guided phototherapy of tumors [38].

In this review, we focus on these fluorescent therapeutic molecules or fluorescent therapeutic aggregates, fluorescent therapeutic nanocomposites based on organic molecular structures, for phototherapy of tumors. According to the different parent structures of organic parents, they are mainly divided into cyanine, tetrapyrrole structure, BODIPY, and AIEgens, which can be used for fluorescence imaging-guided PDT, PTT, and PDT combined PTT against cancers (Fig. 1). In addition, we have in-depth summarized the impact of structural modification (molecular level) or regulated aggregation mode (nano-level) on energy dissipation, providing feasible strategies for constructing PSs that meet both imaging and therapeutic effects. Moreover, we also elaborated on the ways in which molecular structure or nanostructured phototheranostic agents can enhance the effect of phototherapy, which will provide strategies for the subsequent construction of phototheranostic agents with precise tumor imaging and treatment.

2. Design strategy for efficient phototheranostic agents

The Jablonski diagram is the golden rule to guide the design of molecular phototheranostic agents, which modulates its fluorescence, PDT and PTT properties by regulating three main strategies of excitation energy dissipation pathways [20]. As shown in Fig. 2, when a phototheranostic organic molecule absorbs a photon, it will move from the S_0

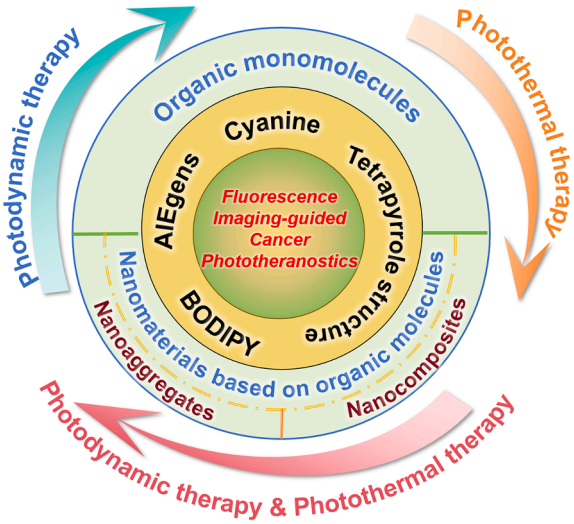

Fig. 1. Schematic illustration of fluorescence imaging-guided cancer phototheranostics.

to the lowest singlet excited state (S_1) that can undergo three different energy dissipation pathways to reach the S_0 Photons with longer wavelength and lower energy released directly from S_1 to S_0 through radiation dissipation are called fluorescence. Phototheranostic organic molecules in the S_1 state can also relax to S_0 through non-radiative vibration, thereby generating heat and causing local temperature increases. PTT refers to this process, which achieves the purpose of tumor ablation through the increase of local temperature. In general, excited state PSs have a short lifetime and can quickly relax from the S_1 back to the S_0. However, PDT requires the phototheranostic organic molecules to cross from the S_1 state to lowest triplet state (T_1). The PS that crosses into the T_1 state has a relatively long life and has ample opportunity to transfer energy to surrounding substances to generate ROS. As a molecule, the excitation energy it absorbs is fixed, so the three molecular dissipation pathways are always competitive [39]. Accordingly, when constructing molecular structures with multiple functions, we need to fully consider the overall needs. For example, to ensure the therapeutic effect we can appropriately reduce the fluorescence intensity of phototheranostic molecules, and only need to ensure that they can be used for *in vivo* fluorescence imaging. For PTT, when the temperature rises to 42 °C, irreversible tissue damage will occur. Maintaining 42–46 °C for 10 min will cause cell necrosis. Therefore, the temperature only needs to be raised to 42 °C to achieve the PTT effect against tumor [40].

In general, based on the Jablonski diagram, by adjusting the photophysical properties of phototheranostic molecules, it will be much easier for scientists to develop a variety of photodiagnostic reagents with superior performance, which promotes the development of the fluorescence imaging-guided cancer phototheranostics.

3. Cyanine-based fluorescence imaging-guided theranostics for cancer therapy

Cyanine structures, mainly including indocyanine green (ICG), pentamethine indolenine cyanine analogs, heptamethine cyanine analogs, etc., are a type of NIR dyes, especially ICG, which is currently the only U.S. Food and Drug Administration (FDA)-approved NIR fluorescent dye for clinical imaging and diagnosis [41]. Cyanine derivatives have high absorption coefficients ($>10^5$ M^{-1} cm^{-1}), excellent biocompatibility, and low toxicity [42]. Additionally, this type of structure has more modification sites, which is conducive to the regulation of the photophysical properties of organic molecules. More importantly, cyanine derivatives possess natural tumor targeting capabilities, which may be promoted by the mediation of organic anion transporting

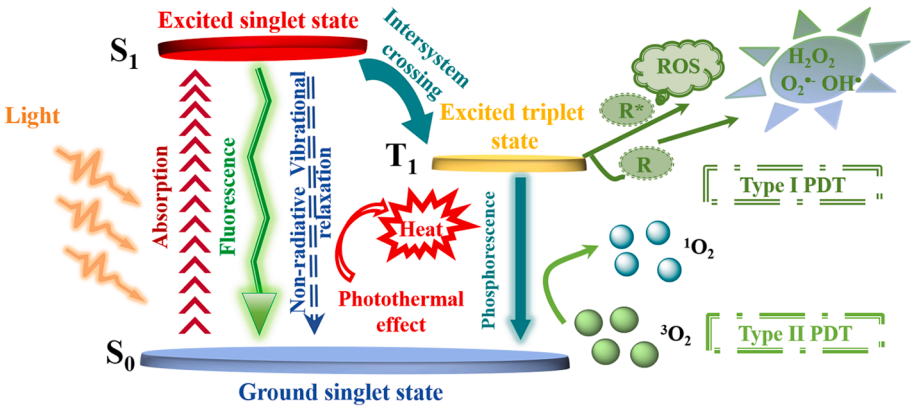

Fig. 2. Schematic of the Jablonski diagram.

polypeptides (OATP) [43]. In view of the above advantages, cyanine molecules, nanoaggregates and nanocomposites constructed based on these cyanine molecules have been widely developed for fluorescence imaging-guided phototherapy of tumors. In this part, we summarize how this type of agents can improve the effect of phototherapy. At the same time, we also list the advantages, disadvantages and other characteristics of some representative structures to provide researchers with a better understanding of the properties based on the cyanine (Table 1).

3.1. Heavy atom effect enhanced PDT

3.1.1. Type II PDT

There are two processes of PDT. When the T_1-state PS exchanges energy with the surrounding O_2 molecules, singlet oxygen ($^1O_2$) will be produced, which is called type II process. The ability of intersystem crossing (ISC) is positively correlated with the effectiveness of PDT. It is reported that adding heavy atoms to the molecular structure will help enhance the possibility of ISC [34,44]. Based on this, a series of heavy-atomized cyanine structures were reported for enhanced PDT. As shown in Fig. 3a, Barbero's group synthesized a series of pentamethyl cyanine dyes by introducing substituent groups including no substituent, iodine, bromine and carboxylic group on the indole ring, which were named CY-C4, I-CY-C4, Br-CY-C4, and COOH-CY-C4. The absorption of these four compounds are in the phototherapeutic window range of 640–670 nm. With 1,3-diphenylisobenzofuran (DPBF) as $^1O_2$ probe, it was concluded that Br-CY-C4 and I-CY-C4 have higher ability to generate $^1O_2$ than these of CY-C4 and COOH-CY-C4 [45]. Typically, methods to modify heavy atoms to enhance $^1O_2$ yield at the expense of reduced fluorescence emission. As shown in Fig. 3b, when IR 783 is mono-iodinated (6a) or di-iodinated (6b), the fluorescence quantum yields (Φ_f) of its fluorescence emission are calculated to be 0.22 and 0.009 respectively, which were both lower than ICG (0.27). Using singlet oxygen sensor green (SOSG) as the indicator, the $^1O_2$ yield of 6a is 7.9 times higher than that of ICG [46]. In order to increase the targeting efficiency, iodinated cyanine is combined with trastuzumab (Ab) to achieve specific identification of the tumor site and enhanced PDT [47].

Table 1
Summary of fluorescence, therapeutic modalities, advantages and disadvantages of representative PSs among cyanine-based molecular or nanomaterials.

Photosensitizer	Fl.	Ther. Mod.	Advantages	Disadvantages	Ref.
heavy-atomized cyanine structures	NIR I	PDT (type II)	broad absorption; enhanced $^1O_2$ generation	Φ_f is relatively reduced; O_2-dependent	[4546]
halogen-modified heptamethine cyanine	NIR I	PDT (type I)	activatable fluorescence; anti-hypoxic PDT; ALP-overexpressed cancer targeting	lower Φ_f (CyI)	[52]
introduced TEMPO into Cy7	NIR I	PDT (type II)	extremely high Φ_Δ and low dark cytotoxicity	weakening of fluorescence	[55]
modification of acetophenone at thiopentamethylcyanine	NIR I	PDT (type II)	enhancement of fluorescence and ROS generation; tumor-targeted imaging	O_2-dependent	[60]
fluorination of a squarylium indocyanine	NIR I	PDT (type II)	enhanced ROS generation; ER-targeting; O_2 supply	the synthesis is relatively complex	[67]
nitro imidazole modified IR-1048 dye	NIR II	PTT	hypoxia-activated PTT; high imaging penetration depth	relatively poor water solubility	[73]
pyrene or TPE modified Cy7	NIR I	PTT	enhanced PCE; improved tumor-targeting	low Φ_f; relatively poor water solubility	[80]
hydrophilic quaternary stereo-specific cyanine and polypeptide based nanoparticles	NIR II	PTT	increased water solubility; improved biocompatibility and PCE	requires relatively high laser intensity	[82]
tamoxifen modified cyanine	NIR I	PTT	breast cancer targeted; enhanced tumor inhibition rate	relatively low fluorescence penetration depth	[86]
biotin modified cyanine	NIR I	PDT & PTT	ratiometric fluorescence; tumor-targeting; pH activated phototherapy	relatively low fluorescence penetration depth and photostability	[102]
dimeric heptamethine cyanine with an aromatic diphenol linker	NIR I	PDT & PTT	bright fluorescence, excellent ROS generation capability; improved photostability	requires relatively high laser intensity; relatively poor water solubility	[103]
nanoaggregates based on twistable TPE structure between two IR780s	NIR I	PDT & PTT	tumor targeting; mitochondria targeted disassembly; high PCE;	relatively poor water solubility	[43]
crizotinib modified IR808 self-assembled with BSA	NIR II	PDT & PTT	excellent biocompatibility and biosafety; colorectal cancer targeting	requires relatively high laser intensity	[116]

Fl., fluorescence; Ther. Mod., therapeutic modalities; Ref., reference; Φ_f, fluorescence quantum yield; TEMPO, 2,2,6,6-tetramethylpiperidinyloxy; Φ_Δ, singlet oxygen quantum yield; TPE, tetraphenylethene; Cy7, heptamethine cyanine; PCE, photothermal conversion efficiency.

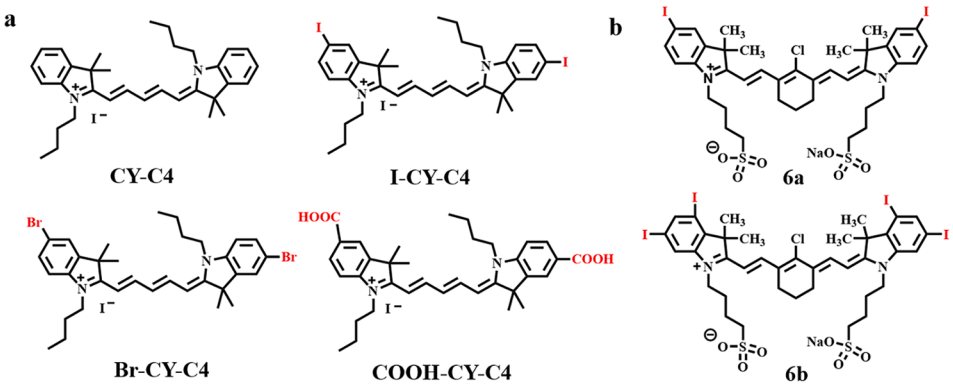

Fig. 3. (a) Chemical structures of CY-C4, I-CY-C4, Br-CY-C4, and COOH-CY-C4. (b) Chemical structures of 6a and 6b.

3.1.2. *Type I PDT*

Tumors, especially solid tumors, have a hypoxic microenvironment due to insufficient O_2 supply and heterogeneity in the vascular network [48]. Compared with O_2-dependent type II PSs, type I PSs are more conducive to the application of hypoxic tumor microenvironments. When the PS that absorbs photons reaches the T_1 state, it undergoes an H- or electron transfer process with the surrounding substrate molecules, generating free radicals or free radical ions such as superoxide anions ($O_2^{\bullet-}$), hydroxyl radicals (•OH), etc.) [49]. Reactive free radicals can oxidize important biomolecules in cells and damage cells through necrosis and/or apoptosis pathways [50]. Among them, •OH originates from the cascade biological reaction of $O_2^{\bullet-}$ (Haber-Weiss/Fenton reaction) or the oxidation of water in the type I process [51]. •OH has extremely high chemical reactivity towards almost all biological molecules and is the most aggressive ROS species.

Generally, heptamethine cyanine has low ROS production capacity. To increase its ROS generation capacity, especially type I-type ROS, Miao and co-woekers introduced halogen to increase the spin–orbit coupling (SOC) constant, thereby having favorable ISC rate. A series of cyanine structures CyH, CyBro, CyBr, and CyI were constructed (Fig. 4a) by introducing and adjusting the positions of halogens (Br and I). The absorption of all molecular structures located in the NIR region from 650 to 800 nm, and the fluorescence emission is between 700 and 850 nm. By calculation, the Φ_f of CyH, CyBro, CyBr, and CyI are 0.21, 0.12, 0.07, and 0.03 respectively. The Φ_f of CyBr, and CyI decreased significantly.

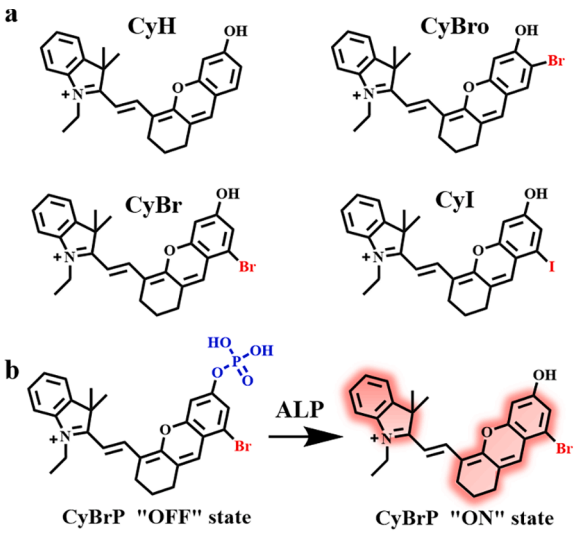

Fig. 4. (a) Chemical structures of CyH, CyBro, CyBr, and CyI. (b) Chemical structures and reaction of CyBrP with ALP.

Using 9,10-anthracenediyl-bis(methylene)dimalonic acid (ABDA) as the $^1O_2$ indicator and DHR 123 as the $O_2^{\bullet-}$ probe, the ROS produced by four molecular structures after illumination were identified. These four molecules hardly produce $^1O_2$, and the ability to produce $O_2^{\bullet-}$ follows the following order: CyH < CyBro < CyBr < CyI, proving that the production of $O_2^{\bullet-}$ is effectively increased by introducing halogen atoms. Taking into account the two effects of fluorescence and PDT, they chose CyBr as the phototheranostic agent. A phosphate group that can be activated by alkaline phosphatase (ALP) which is overexpressed in tumors was further introduced into the CyBr to construct a non-fluorescent and non-phototoxic CyBrP. After CyBrP reacts with ALP, CyBr can be released, thereby restoring its fluorescence and phototoxicity (Fig. 4b) [52].

3.2. *Heavy atom-free effect enhanced PDT*

The introduction of heavy atoms into PSs can increase the PDT effect. However, it will lead to an increased dark toxicity, thus limiting their biological applications [53,54].

To avoid the impact of introducing heavy atoms to increase dark toxicity on biological applications, Peng et al. introduced 2,2,6,6-tetramethylpiperidinyloxy (TEMPO) into the middle of the Cy7 structure to construct dye 2 (Fig. 5a) for enhanced ISC process, thereby increasing the production of ROS. Dye 2 has high singlet oxygen yield (0.20) and low dark toxicity (IC_{50} = 715.4 μM) [55]. Modification in the cyanine position increases the ISC effect and often weakens the dissipation of excited state energy through fluorescence [56]. In order to avoid excessive weakening of fluorescence, Du et al. achieved the preparation of C2-R (R = NO_2, CF_3, COOH, H, OMe, NH_2) series compounds (Fig. 5b) by using acetophenone at the C2′ position of the thiopentamethyl cyanine (TCy5). Through the modification on the C2′ aryl group, the photoinduced electron transfer (PET) of the compound is controlled to enhance ISC, and the compound fluorescence is adjusted according to the twisted intramolecular charge transfer (TICT) [57,58]. By combining TICT and PET, the competitive relationship between fluorescence and triplet states can be overcome, which can help to achieve simultaneous enhancement of fluorescence and ROS generation. After experiments, the absolute Φ_f of six compounds were obtained as 4, 18, 20, 28, 35, 32 respectively, while the relative singlet oxygen quantum yield ($\Phi_{\Delta rel}$, ICG as standard) were 6.0, 9.3, 10.8, 13.2, 16.4, and 24.3, respectively (Fig. 5c and 5d). Considering Φ_f and $\Phi_{\Delta rel}$, C2-NH_2 has optimal photophysical and chemical properties. Nitroreductase (NTR), highly expressed in hypoxic tumor cells that can convert nitro groups into amino groups [59]. Low fluorescence and phototoxic C2-NO_2 was selected as the phototheranostic agent, which can be converted into C2-NH_2 under hypoxic conditions to restore fluorescence and the production of ROS (Fig. 5e). In vivo whole-body imaging experiments show that C2-NO_2 exhibits excellent tumor-targeted imaging capabilities in 4T1

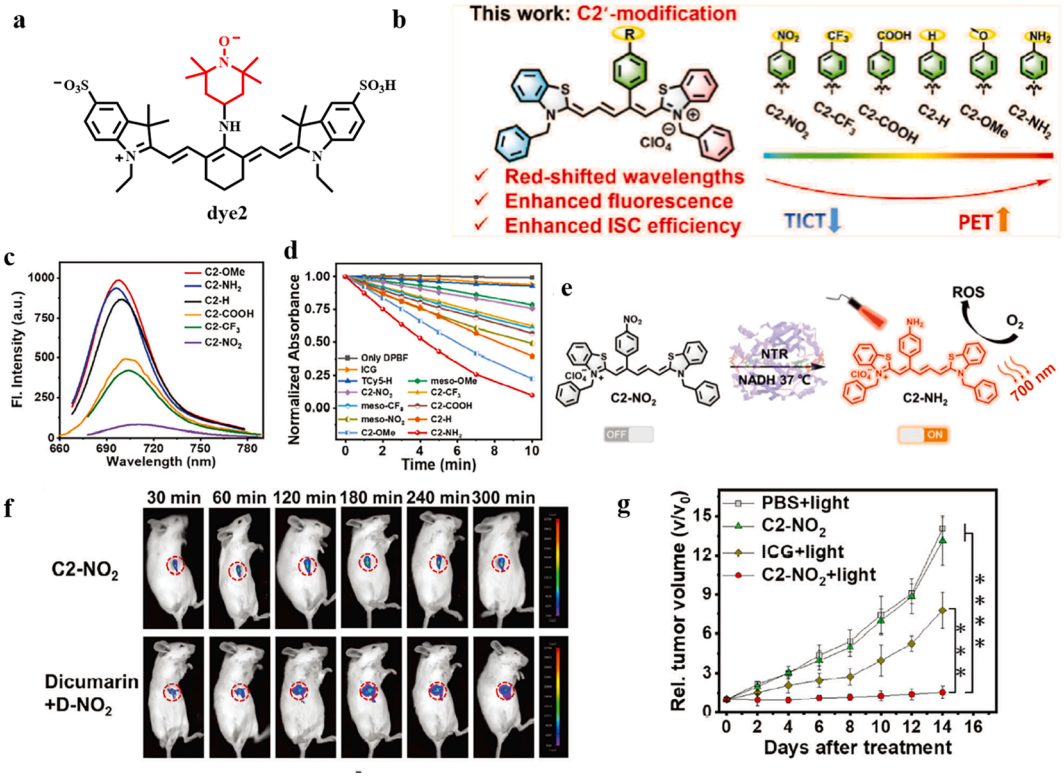

Fig. 5. (a) Chemical structure of dye 2. (b) Chemical structures of C2-R. (c) Fluorescence emission spectra of the various dyes in DCM. (d) Normalized DPBF absorbance decrease at 415 nm. (e) The reaction of C2-NO_2 to C2-NH_2 in the presence of NTR. (f) Fluorescence imaging of tumor-bearing mice after different treatments. (g) Relative tumor volume of mice over time after different treatments. Reprinted with permission from Ref. [60], copyright © 2023 The Authors. Advanced Science published by Wiley-VCH GmbH.

tumor bearing mice (Fig. 5f). As shown in Fig. 5g, after exposure to light, the tumor growth was significantly inhibited [60].

In addition to the hypoxic microenvironmental natures, tumors are also characterized by weak acidity and high thiol content. Constructing a specific response structure based on the characteristics of the tumor microenvironment is of great significance for targeted imaging and treatment of tumors [61]. Cai and co-workers achieved dual thiol/pH sensing by combining 5′-carboxy rhodamine (Rho) and heptamethine cyanine IR765 (Cy) with a reducible disulfide bond and a pH-adjustable amino group. The synthetic compound RhoSSCy (Fig. 6a) enables targeted imaging and treatment of tumors [62].

ROS produced by PDT have a 0.03 − 0.18 ms short lifetime in biological systems and a limited diffusion distance about 0.01 − 0.02 μm [63]. Therefore, the production site of ROS is directly at the “death site” of tumor cells, which is more conducive to obtaining positive anti-tumor effects. Lysosomes play an important role in substrate degradation, cell signaling, and activation of apoptosis and necrosis [63]. Sun et al. constructed three molecular structures (HCL1-3, Fig. 6b) by modifying piperazine and N,N-dimethyl structures on heptamethocyanine to achieve enhanced phototherapy effects by targeting lysosomes [64].

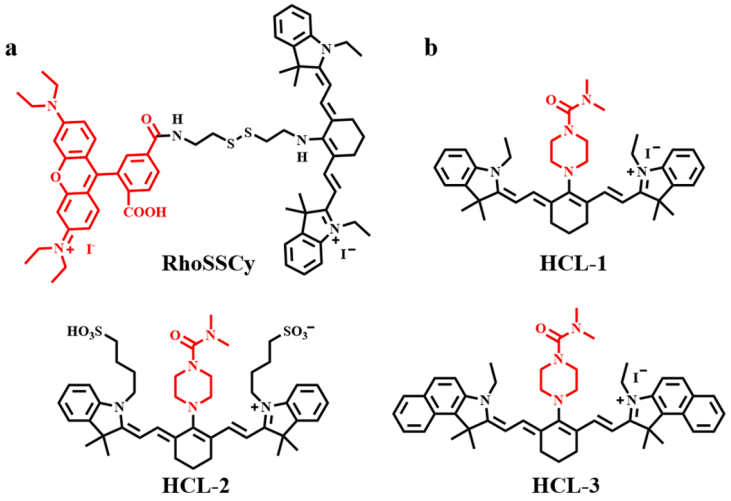

Fig. 6. Chemical structures of (a) RhoSSCy and (b) HCL1-3.

3.3. Overcome tumor hypoxia enhanced PDT

Tumor hypoxia generally occurs in deep-seated tumors and the hypoxic condition severely limits the effect of PDT especially the type II process and may even increase tumor metastasis and recurrence [65]. To overcome the bottleneck of PDT, researchers have conducted a series of studies on the characteristics of hypoxic microenvironments. Compared with single-molecule structures, nanoplatforms have the advantages of enhanced penetration and retention (EPR) effect, thereby improving the ability to passively accumulate at tumor sites; as well as low toxicity and the integration of multiple functions [62]. Peng's group constructed a multifunctional nanoprodrug Mal@Cy-NTR-CB (Fig. 7a), in which Cy-NTR-CB serves as a functional part of fluorescence imaging, PDT, and chemotherapy. In the specific hypoxic and high NTR condition of the tumor, Cy-NH_2 can be released, which can be used for fluorescence and PDT are released. Maleimide (Mal) in the nanostructure can regulate the content of glutathione (GSH), prevent the clearance of $^1O_2$, and achieve high therapeutic efficiency of PDT [66].

Two commonly used strategies are used for improving the phototherapy effect of hypoxic tumors: (1) Alleviate tumor hypoxia by carrying ample O_2 for PDT; (2) Construct non-oxygen-dependent type I PSs to ensure the therapeutic effect while reducing O_2 consumption. Yin et al. designed and synthesized the amphiphilic phototherapeutic molecule Fcy (Fig. 7b) based on squaryl indocyanine dye skeleton linked to perfluorooctane and PEG-biotin. Fcy self-assembles into FCy NPs in aqueous solution, and the nanostructured FCy NPs owned the following advantages: (1) The aggregation of squaraine structures increases the ability of ISC, thereby improving ROS production capacity; (2) The presence of perfluoroalkyl groups, which have excellent O_2 carrying capacity and endoplasmic reticulum targeting ability; (3) The presence of biotin improved the tumor targeting ability. This multi-functional FCy NPs exhibit excellent anti-tumor ability [67].

Through host–guest interaction, reducing the π–π stacking of phototheranostic agents and inhibiting mitochondria-related oxidative phosphorylation (OXPHOS) to promote more O_2 for PDT is also an effective strategy for hypoxic tumors [65]. Gasser's group connected symmetric heptamethine cyanine dyes to Ru(II) polypyridine complexes through phenanthrimidazole ligands to construct NIR-activatable PSs strategy. This series of synthesized compounds are named Ru-Cyn-1, Ru-Cyn-2, Ru-Cyn-3, and their specific structures are shown in Fig. 7c. Among them, Ru-Cyn-1 has type I and type II photodynamic properties under 770 nm laser irradiation, and can kill tumors under normoxic and hypoxic (2 % O_2) conditions.

3.4. Activatable properties for enhanced PTT

Currently, most of the phototheranostic agents generally show "always on" fluorescence and photoactivity. This can easily cause non-tumor cells to be "accidentally injured" after being illuminated, increasing the side effects of phototherapy [4]. Activatable phototheranostic agents that can be activated by the tumor microenvironment and then "turn on" the therapeutic effect, which is of great significance for the precise treatment of tumors.

A type of "Dual-Key-and-Lock" asymmetric cyanine structures named Cy-830, NSCy-975, NSCy-980 and NSCy-1015 for the diagnosis and treatment of liver diseases were designed and synthesized by Xiong and co-workers. The detailed structure and response strategy are shown in the Fig. 8a. NSCyanine has a pKa < 4.0 and exhibits weak fluorescence in acidic lysosomes (key1); when intracellular viscosity increases, strong fluorescence is restored (key2). Among them, NSCy-1015, which has camptothecin (CPT, anti-cancer drug) modified through a disulfide bond, is used for tumor ablation. The abundant GSH in the tumor breaks the disulfide bond to release CPT, while the protonation of the N atoms of the indole moiety and the increase in intracellular viscosity activate the NIR II fluorescence of NSCyH-1015 (Fig. 8b). Compared with the NIR I, the fluorescence imaging of the second near-infrared window (NIR-II, 900–1700 nm) can reduce the interference of tissue autofluorescence, and has a deeper penetration depth and higher spatial resolution [68,69]. The results of whole-body and *in vitro* organ NIR II fluorescence imaging of 4T1 tumor-bearing mice indicated that NSCy-1015 gradually accumulated at the tumor site after tail vein injection. At 48 h after injection, NIR II fluorescence was almost only observed at the tumor site (Fig. 8c and 8d). After 6 min of 808 nm laser irradiation, the temperature of the tumor site rose to 56 °C (0.75 W/cm^2), which has good tumor elimination ability (Fig. 8e and 8f) [70].

Hypoxia can cause the overexpression of NTR, and the expression level of NTR is related to hypoxia. Therefore, NTR can be known as a marker of hypoxia, and its expression level can be used to evaluate the degree of hypoxia in tumors [71,72].

Cai et al. designed and synthesized an NTR enzyme-responsive NIR II phototheranostic agent IR1048-MZ by modifying the 2-(2-nitroimidazolyl)ethylamine (MZ) onto the IR-1048 skeleton (Fig. 9a). The electron-withdrawing MZ group induces electron transfer, causing quenching of fluorescence and a decrease in absorbance of IR-1048. When MZ is reduced to the corresponding amine by NTR, the NIR fluorescence recovers, the absorption increases, and the PTT effect is enhanced [73].

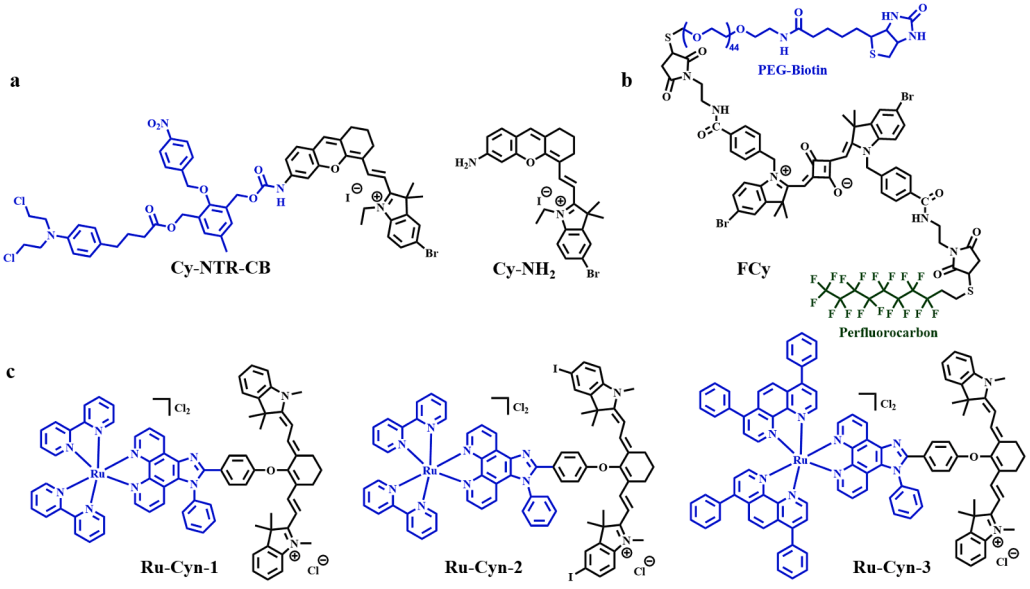

Fig. 7. Chemical structures of Cy-NTR-CB and Cy-NH_2 (a), FCy (b); Ru-Cyn-1, Ru-Cyn-2, Ru-Cyn-3 (c).

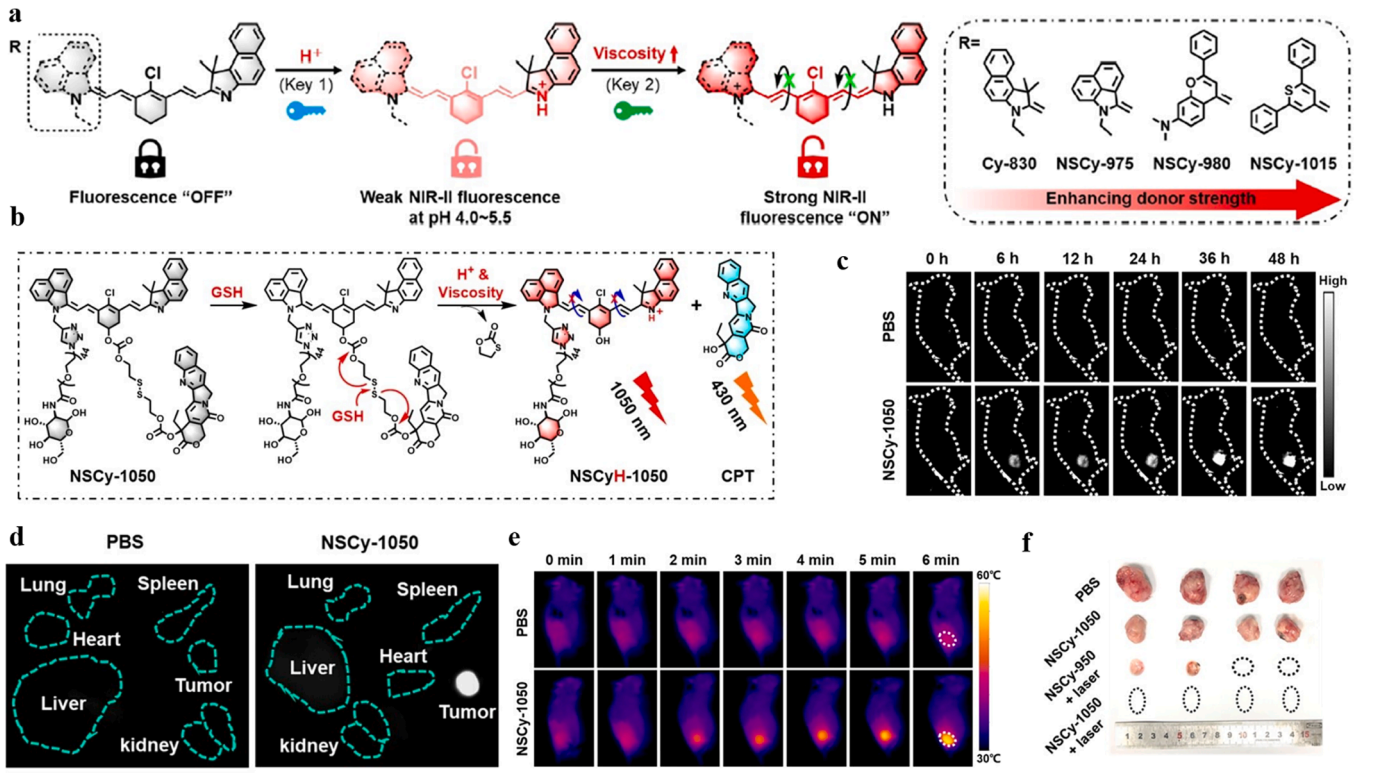

Fig. 8. (a) Chemical structures of Cy-830, NSCy-975, NSCy-980 and NSCy-1015 and their design stratagem; (b) The response mechanism of NSCy-1050; (c) Time-dependent whole-body NIR-II fluorescence imaging of 4T1 tumor-bearing mice after *i. v.* injection of NSCy-1050; (d) *Ex vivo* NIR-II fluorescence imaging of organs; (e) *In vivo* photothermal images of 4T1 tumor-bearing mice after laser irradiation various times; (f) Photographs of the tumors from different groups after therapy. Reprinted with permission from Ref. [70], copyright © 2023 Wiley-VCH GmbH.

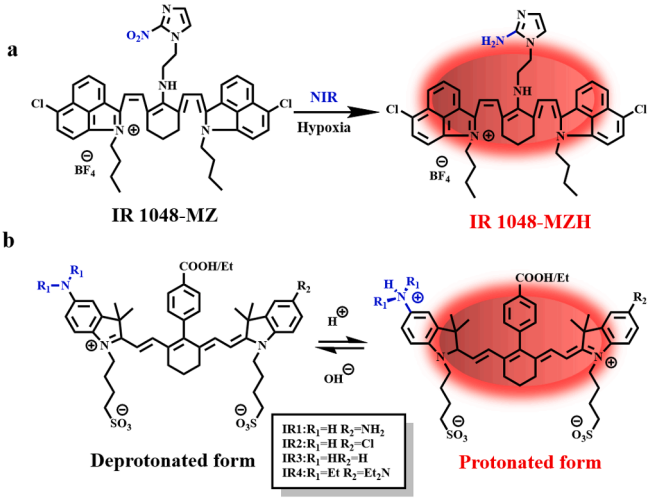

Fig. 9. (a) Chemical structure and response mechanism of IR1048-MZ; (b) Chemical structures of IR1-IR4 and the response mechanism of them.

The difference in pH between tumor cells and normal cells is also one of the methods used to design tumor-activated phototheranostic agent. Li's group replaced the benzoic acid group at the middle position of IR 783 (to improve photostability), and introduced an amine group (electron-donating) at the 5-position of the terminal indole ring as pH responsive group to construct IR1-IR4 (Fig. 9b). The fluorescence intensity of these four compounds changes as the pH modifies. Among them, IR2 has a PKa of 4.6 and can light up acidic lysosomes and selectively eliminate cancer cells by maximizing the PTT effect in alkaline mitochondrial matrices [74].

3.5. Regulation the aggregation state for enhanced PTT

The cationic character of the cyanine promotes its aggregation in salt solutions through electrostatic interaction. Compared with cyanine monomers, the absorption and emission bands of J-aggregates will be red-shifted, thus promoting better fluorescence efficiency [75,76].

Yang et al. designed a Cy-CO_2Bz structure containing N-benzyloxycarbonyl group, which can self-assemble into J-aggregates in the presence of NaCl (Fig. 10a). The J-aggregate absorbs at 890 nm, and after exposure to light, the PCE increases from 29.37 % to 57.59 % [77].

According to Kasha excitonic coupling theory, H aggregation has

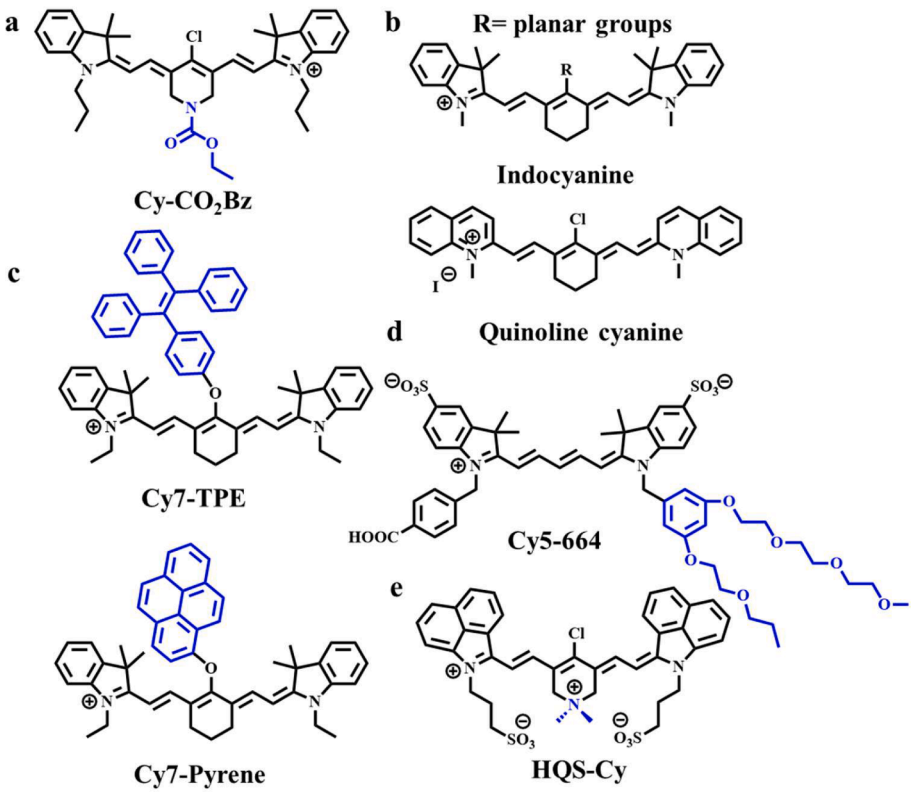

Fig. 10. (a) Chemical structure of Cy-CO_2Bz; (b) Chemical structures of Indocyanine and Quinoline cyanine; (c) Chemical structures of Cy7-TPE and Cy7-Pyrene; (d) Chemical structure of CY5-664; (e) Chemical structure of HQS-Cy.

more internal transformation and vibrational relaxation trends than J aggregation, which makes it easier to generate heat for PTT [78]. Yin and co-workers designed quinoline cyanine (QCy) organic molecules to construct stable H-aggregated nanomaterials (QCy NPs), achieving high stability and high photothermal conversion rate (Fig. 10b), from 20.1 % (non-H-aggregated QCy) to 63.8 % (QCy NPs) [79]. Li et al. introduced a pyrene or tetraphenylethene (TPE) structure into the central position of heptamethine cyanine named Cy7-TPE and Cy7-Pyrene to construct self-assembled nanomaterials through H aggregation for enhanced PTT (Fig. 10c) [80].

Although H-aggregated self-assembled nanomaterials exhibit excellent PTT efficiency, they often lead to extremely low fluorescence quantum yields and reduce the accuracy of fluorescence imaging. Therefore, some researchers have enhanced their fluorescence and PTT effects by increasing the water solubility of compounds or nanoparticles and increasing their absorption in aqueous solutions. Zhang et al. used a water-soluble pentamethylocyanine analog, 1-(4-carboxybenzyl)-2,3,3-trimethylindoleninium-5-sulfonate bromide (CY5-664, Fig. 10d), for fluorescence imaging-guided PTT [81].

To further increase hydrophilicity and improve biological applications, Yan's group synthesized a NIR II cyanine (HQS-Cy) structure with quaternary stereospecificity as shown in Fig. 10e. In terms of molecular structure, the water solubility is increased by introducing sulfonic acid groups, and the dimethylammonium functional group prevents the aggregation of HQS-Cy through charge-charge mutual repulsion; at the nanometer level, HQS-Cy@P NPs is constructed by encapsulating HQS-Cy with amphiphilic polypeptides. The absorption and emission of HQS-Cy@P NPs are both located in the NIR II range (absorption 980 nm; emission 1050 nm) and the PCE can reach 35.5 % [82].

3.6. Tumor or/and subcellular organelle-specific targeted enhanced PTT

Tumor-specific targeting is an effective strategy to enhance diagnosis and treatment and reduce damage to adjacent cancer tissues. Targeting of tumor tissue is mainly divided into two categories. One is passive targeting, which achieves EPR effect at the tumor site by adjusting the particle size and surface structure of nanomaterials or macromolecules [83]. The other type is active targeting, which mainly binds high-affinity ligands to specific surface molecules overexpressed by cancer cells or tumor epithelial cells, such as proteins, aptamers, peptide chains, etc [4]. High expression of estrogen receptor (ER) is generally associated with breast cancer [84]. Tamoxifen (TAM) is a targeted drug for ER^+ breast cancer that can inhibit the growth and proliferation of breast cancer cells [85].

CyT, a compound covalently linked to TAM on the Cy parent structure, was successfully constructed by the Fan' group (Fig. 11a) for enhanced phototherapy of breast cancer with high ER-expression and mitochondrial targeting (the cationic properties of Cy endow it with mitochondrial targeting ability). Compared with Cy that lacks TAM, CyT exhibits excellent tumor targeting ability, and its fluorescence intensity in tumors is significantly higher than that of Cy group (Fig. 11b and 11c). After illumination (808 nm, 0.8 W cm^{-2}), the temperature increase in the CyT group was significantly higher than that of Cy group (Fig. 11d), and the CyT group showed the best tumor inhibition rate (Fig. 11e) [86].

Different from the above, Tang et al. constructed the Met-IR-782 molecule by modifying methionine (Met) on the middle structure of IR 782 to achieve specific human breast adenocarcinoma cell line (MCF) NIR fluorescence imaging and eradication (Fig. 12a) [87].

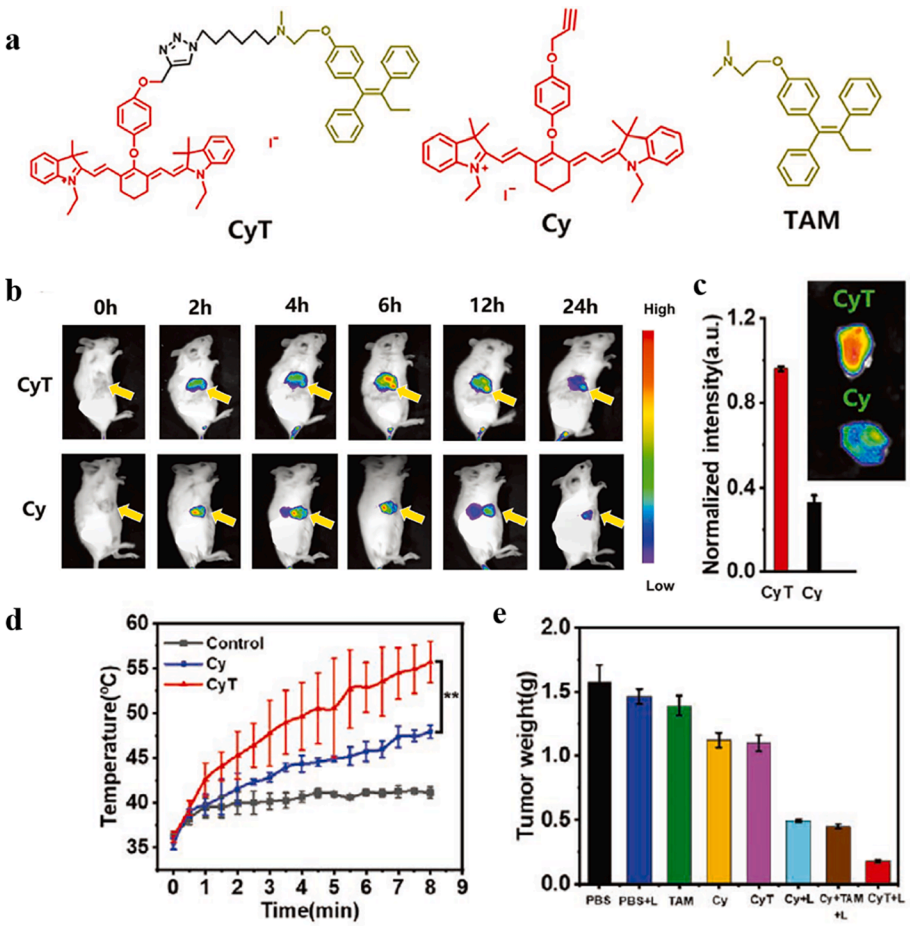

Fig. 11. (a) Chemical structure of CyT, Cy and TAM; *In vivo* (b) and *ex vivo* (c) fluorescence imaging of tumor-bearing mice (b) and tumors (c) with different treatments. (d) Time-depended temperature changes at the tumor sites after laser irradiation. (e) Tumor weight of tumor-bearing mice with different treatment. Reprinted with permission from Ref. [86], copyright © 2020 WILEY-VCH Verlag GmbH & Co. KGaA, Weinheim.

Cyanine structures have intrinsic tumor targeting ability, which relies on the mediation of OATP. Based on the advantages of cyanine structures, Cai and co-workers constructed IR-PY based on the IR-822 skeleton covalently connected to the pH-responsive N1-(pyridin-4-ylmethyl)ethane-1,2-diamine (PY) group to achieve tumor specific "turn on" NIR fluorescence imaging and PTT (Fig. 12b) [88].

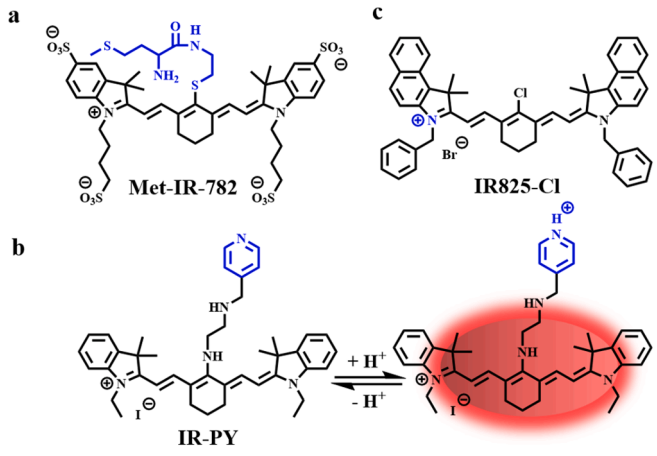

Fig. 12. (a) Chemical structure of Met-IR-782; (b) Chemical structure of response mechanism of IR-PY and its reaction in different pH; (c) Chemical structure of IR825-Cl.

Besides, the cationic nature of the cyanine structure gives it the ability to target mitochondria. Chen et al. designed and synthesized a mitochondria-targeted IR825-Cl structure for mitochondria-targeted phototherapy of tumors (Fig. 12c). Interestingly, IR825-Cl exhibits fluorescence quenching in aqueous solution, but in mitochondria, a 552 nm laser can be used to emit red fluorescence (emission at 610 nm), while the photothermal effect requires 808 nm light excitation, thus retaining the fluorescence ($\Phi_f > 43$ %) and PTT effect (PCE 17.4 %) [89]. To improve the passive targeting ability of tumors, a series of photothermal agents with fluorescence imaging functions are self-assembled with polymer or biological carriers BSA/HSA to construct nanoparticles with improved biocompatibility and tumor targeting ability [90,91].

3.7. Other methods for enhanced PTT

The poor photostability and relatively low PCE limit its application in PTT. Controlling the photophysical and chemical properties of cyanine compounds by introducing metal ions is a feasible strategy. Lin and co-workers synthesized terpyridine-grafted nitrogen-terminated Cy7 precursor (CydtPy) and chelated it with metal ions Mn^{2+}, Fe^{2+}, etc. to control the photophysical properties. Compared with CydtPy, the fluorescence emission intensity of Mn^{2+}-chelated CydtPy increases significantly; after chelating with Fe^{2+} it showed the boosted the photostability and PCE (Fig. 13) [92]. Lin et al. found that when Gd metal and IR1064 were co-assembled in aqueous solution to form Gd@IR1064, Gd@IR1064 did not exhibit a blue shift of the maximum absorption

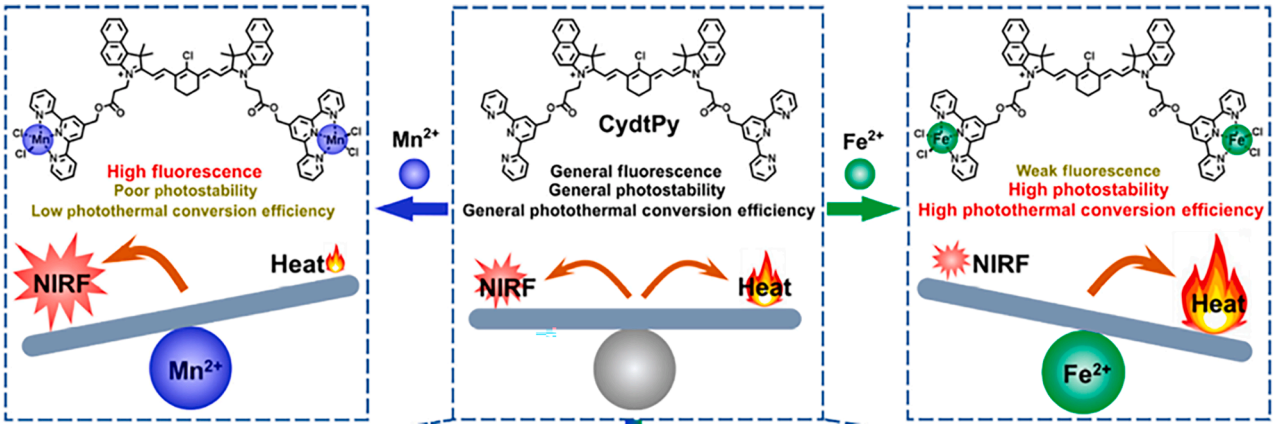

Fig. 13. Chemical structure, photophysical and chemical properties of CydtPy, Mn^{2+}-chelated CydtPy and Fe^{2+}-chelated CydtPy. Reprinted from Ref. [92], copyright © 2023 Junfei Zhu et al. Distributed under a CC BY 4.0.

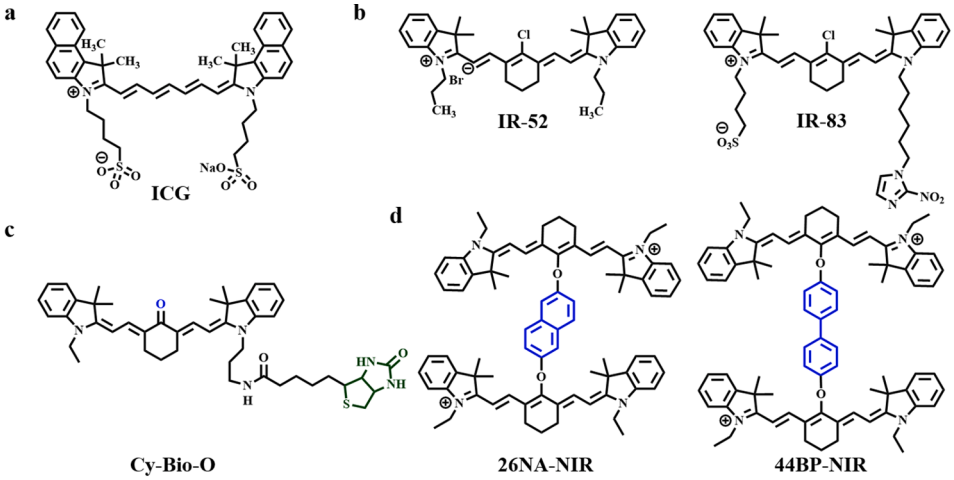

Fig. 14. Chemical structures of ICG (a), IR-52 and IR-83 (b), Cy-Bio-O (c), 26NA-NIR and 44BP-NIR (d).

spectrum or quenching of fluorescence, while other metals such as Mn^{2+}, Fe^{3+}, Cu^{2+}, Mg^{2+}, Zn^{2+}, Al^{3+} do not have this property. Researchers speculate that this is likely caused by IR1064 mitigating π-π stacking in the presence of Gd^{3+}. Therefore, Gd@IR1064 can be used for NIR II fluorescence imaging-guided PTT [93].

3.8. Molecule structure for combined PDT and PTT

The hypoxic tumor microenvironment limits the efficiency of PDT, and high GSH in the tumor consumes ROS and weakens the effect of PDT. The O_2 consumed during PDT is difficult to replenish in time, which aggravates the hypoxia of the tumor [94]. PTT generally requires higher light intensity, and the PS needs to have relatively high PCE to achieve a temperature of > 42 °C that has a killing effect on tumors.

The combined use of PDT and PTT, the thermal effect generated during the PTT process is beneficial to increase the penetration of O_2 into the tumor site and alleviate the hypoxia of the tumor. Also, ROS generated during the PDT process can also help alleviate the weakening of the PTT effect caused by the upregulation of heat shock proteins [95].

ICG (Fig. 14a) is the FDA-approved NIR reagent for clinical imaging [96]. Also, ICG can also be used for fluorescence imaging-guided photodynamic and photothermal synergistic therapy of liver cancer cells [97]. In order to increase the photodynamic and photothermal therapeutic effects of ICG analogs and ensure that their fluorescence properties can be used for *in vivo* imaging, heavy atomic iodine was introduced into the ICG analog Cy7 to meet the purpose of imaging-guided phototherapy [98]. Expect ICG, some heptacyanine derivatives are also used as fluorescence imaging-guided PDT and PTT therapeutic agents, such as IR-52 and IR-83 (Fig. 14b) [99,100]. The lipophilic cation is modified through the N-alkyl side chain on the submethyl core, Shi's group constructed a series of cyanine derivatives (1–27) for fluorescence imaging-guide mitochondrial targeting phototherapy [101].

To increase the tumor cell targeting and responsiveness of tumor pH, Cy-Bio-O with ratiometric fluorescence properties was designed and synthesized by Li et al. The specific structure is shown in Fig. 14c. The fluorescence emission of Cy-Bio-O itself is at 645 nm. Under acidic conditions, the fluorescence emission red-shifts to 758 nm and the photodynamic and photothermal properties of Cy-Bio-O are stimulated [102].

To enhance the phototherapy effect guided by NIR fluorescence and balance the influence of excited state energy dissipation on fluorescence, photodynamic and photothermal effects, Sun and co-workers designed and synthesized a series of dimeric heptamethonine structures. The mid-substituted chlorine atom is replaced by an oxygen atom to increase the molar extinction coefficient and improve the light absorption capacity [80].

Connecting different conjugated aromatic rings via aromatic diphenol linkers increases π-conjugation and push–pull electronic effects. With the steric hindrance and rigidity of the structure increase, reducing intermolecular interactions and achieving a balance between radiative and non-radiative energy dissipation. Through the property determination of a series of compounds, both the 26NA-NIR and 44BP-NIR

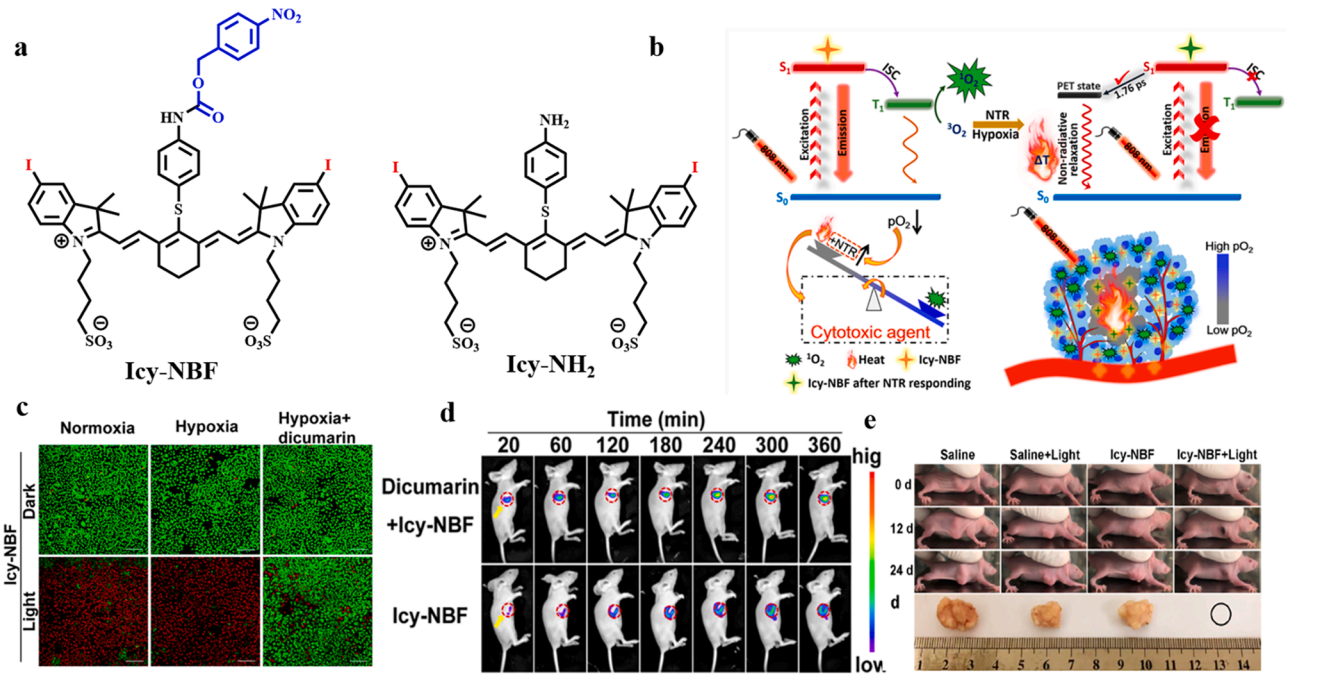

Fig. 15. (a) Chemical structures of Icy-NBF and Icy-NH_2. (b) Schematic illustration of O_2-dependend energy dissipation. (c) Confocal imaging of calcein-AM and PI-labeled Hela cells with different treatments. (d) *In vivo* fluorescence imaging of tumor-bearing mice with Icy-NBF. (e) Photographs of mice in the different groups after 0, 12, and 24 days treatment. Reprinted with permission from Ref. [105] (b-e), copyright © 2020, American Chemical Society.

structures (Fig. 14d) demonstrated excellent fluorescence imaging, ROS production, and high PCE [103].

O_2 plays an important role in the PDT process. However, due to the uncontrolled proliferation of cancer cells and insufficient blood supply, the O_2 concentration in solid tumors varies depending on the location. Generally, the O_2 concentration at the edge is higher than deep inside the solid tumor [104]. Fan et al. designed an intelligent phototheranostic agent named Icy-NBF based on the cyanine structure, which can regulate the activation and deactivation process according to O_2 content. Icy-NBF will be reduced to Icy-NH_2 with the same skeleton in the presence of NTR overexpressed hypoxic tumor cells (Fig. 15a). Under the irradiation of 808 nm laser, Icy-NBF mainly undergoes radiative transition and energy transfer, while Icy-NH_2 mainly undergoes non-radiative relaxation. That is, the phototherapy process of Icy-NBF after illumination can switch between PDT and PTT (Fig. 15b). PDT is more likely to occur near the tumor, and PTT is more likely to occur inside the tumor. The results of calcein-AM and PI-labeled staining indicated that after Hela cells are incubated with Icy-NBF and exposed to light, cell death can be caused under both normoxic and hypoxic conditions (Fig. 15c). The results of whole-body fluorescence imaging of tumor-bearing mice show that Icy-NBF can selectively image the tumor site and show good tumor elimination effect after light treatment (Fig. 15d and 15e) [105].

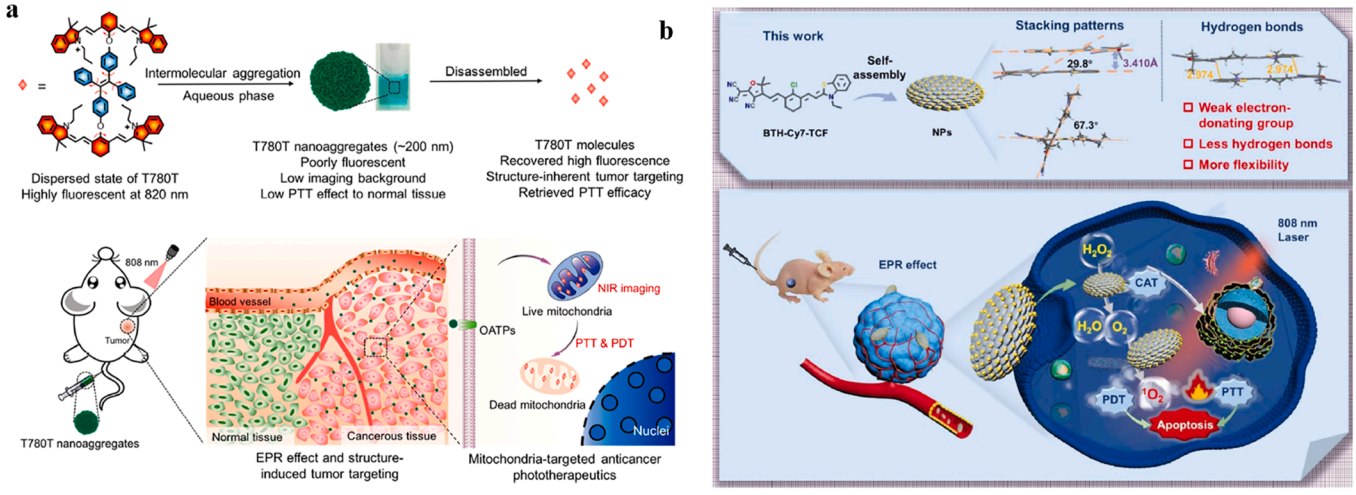

Fig. 16. (a) Chemical structure and its nanoaggregates of T780T; schematic illustration of the application of T780T nanoaggregates in tumor. Reprinted with permission from Ref. [43], copyright © 2021, American Chemical Society. (b) Chemical structure and its self-assembly of BTH-Cy7-TCF; schematic illustration of the application of BTH-Cy7-TCF NPs in tumor. Reprinted with permission from Ref. [110], copyright © 2023 Wiley-VCH GmbH.

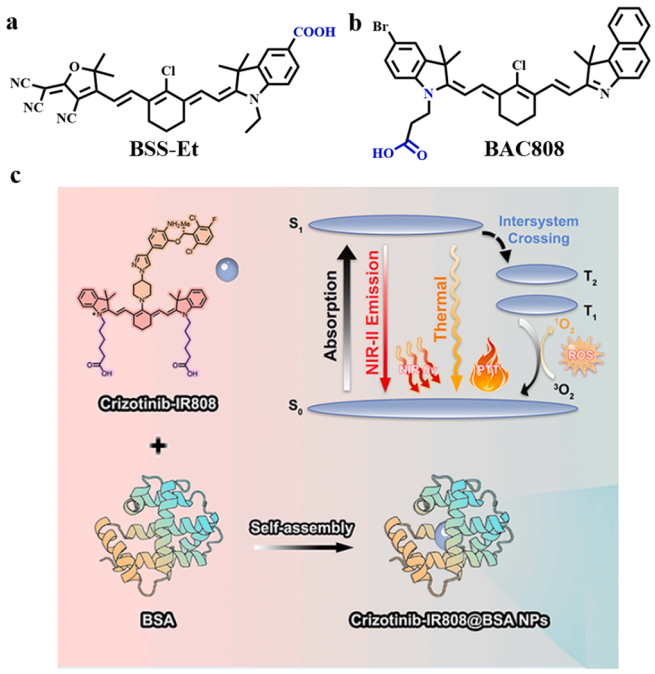

Fig. 17. Chemical structures of (a) BSS-Et and BAC808 (b). (c) The chemical structure of Crizotinib-IR808 and its self-assembly. Reprinted with permission from Ref. [116], copyright © 2023, American Chemical Society.

Table 2
Summary of fluorescence, therapeutic modalities, advantages and disadvantages of representative PSs among tetrapyrrole structures-based molecular or nanomaterials.

Photosensitizer	Fl.	Ther. Mod.	Advantages	Disadvantages	Ref.
morpholine modified SiPc	NIR I	PDT (type I)	pH activatable fluorescence; anti-hypoxic PDT; improved biocompatibility	one-time treatment effect is relatively poor	[121]
lipid-modified porphyrin-based nanomaterials	NIR I	PDT (type II)	hypoxia relief; highly fluorescence; inhibit tumor growth and liver metastasis	preparation of nanomaterials is relatively complicated	[123]
DNBS and cRGD graft onto ZnPc	NIR I	PDT (type II)	enhanced tumor targeting; activatable fluorescence and ROS	relatively poor water solubility	[131]
modifying biotin on SiPc	NIR I	PDT (type II)	enhanced tumor targeting	easy to aggregate	[133]
4-sulfophenoxy mono-α-substituted ZnPc	NIR I	PDT (type II)	turn-on fluorescence; tumor targeted imaging	O_2-dependent	[147]
co-assembly of ZnPc and anti-cancer drug MA	NIR I	PDT (type II)	nucleic acid-responsive fluorescence and ROS; improved anticancer effect	O_2-dependent	[152]
self-assembly peptide modified ZnPc	NIR I	PDT & PTT	photoactivity changes before and after transmembrane	reduced fluorescence intensity	[156]

Fl., fluorescence; Ther. Mod., therapeutic modalities; Ref., reference; SiPc, silicon phthalocyanine; ZnPc, zinc (II) phthalocyanine; DNBS, 2,4-dinitrobenzene sulfonic acid; cRGD, cyclic arginine-glycine-aspartic acid; MA, mitoxantrone.

3.9. Nanomaterials based on small molecule structures for combined PDT and PTT

Nanotheranostic agents can integrate multiple functional units into one nanostructure and have the advantages of extended circulation half-life, low toxicity, etc., which are conducive to the accurate diagnosis and treatment of tumors [62]. In view of the limitations of ICG such as its weak photostability, a variety of nanocarriers are used to deliver ICG to tumor site, including liposomes [106], polyethylene glycolation (PEGylation) [107], inorganic nanomaterials and metal–organic frameworks (MOF) materials, etc [108,109].

IR780 structure exhibits natural tumor targeting ability, but its photophysical and chemical properties in aqueous solution limit its biological applications. Meng's team bridged a twistable tetraphenylethene (TPE) structure between two IR780s and named it T780T. T780T will form uniform T780T nanoaggregates with a particle size of about 200 nm in aqueous solution. The T780T nanoaggregates have low fluorescence and PTT efficiency, which reduces the fluorescence background of normal tissues and the side effects from high heat (Fig. 16a). The T780T nanoaggregates are enriched in tumor cells and targeted to mitochondria to achieve disassembly and restore their fluorescence and therapeutic properties, with a PCE as high as 38.5 % [43]. Zhou et al. synthesized NIR heptamethine cyanine BTH-Cy7-TCF and IND-Cy7-TCF by using tricyanofuran (TCF) as acceptor and benzothiazole (BTH)/indole (IND) as donor. Since the number of hydrogen bonds in BTH is less than that of IND, this reduces the hydrogen bonds and intermolecular π–π interactions of BTH-Cy7-TCF molecules, making BTH-Cy7-TCF aggregates more $^1O_2$ quantum yield (1.3 % vs 0.2 %) and high PCE (56.4 % vs 62.3 %) than that of IND-Cy7-TCF aggregates (Fig. 16b) [110].

Cyanine organic molecules often suffer from poor water solubility. Their solubility is usually improved by introducing charged sulfonates or carboxyl groups. However, this charged structure can interact with biomolecules and hinder their biological application [36]. To further improve the solubility, biocompatibility, tumor-specific targeting ability

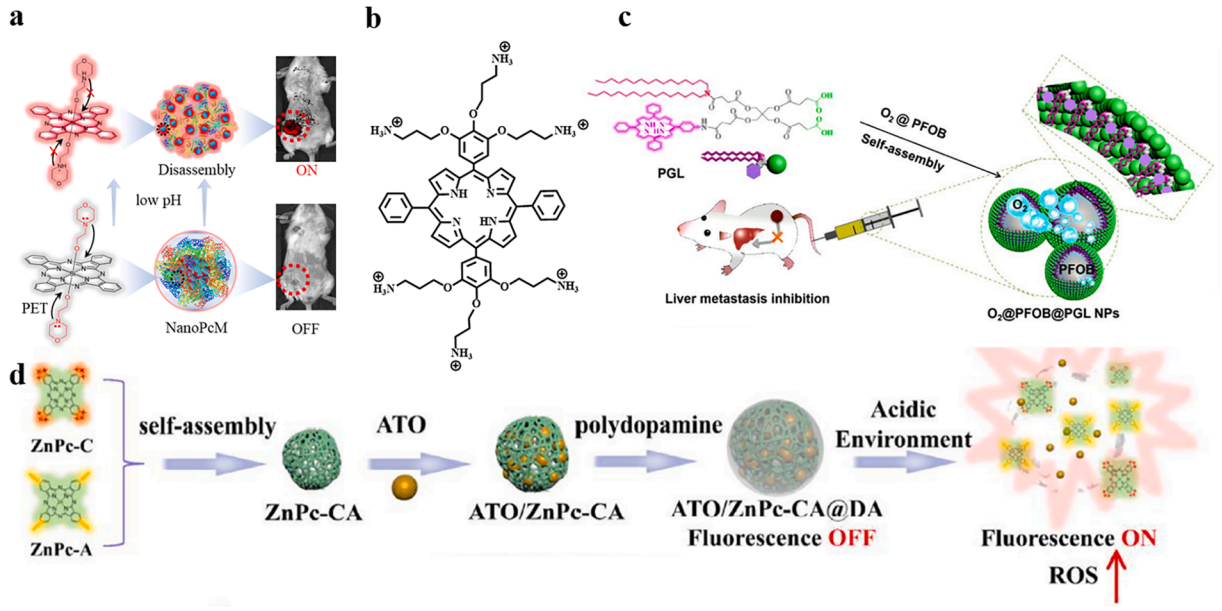

Fig. 18. (a) Chemical structures of PcM and NanoPcM. Reprinted with permission from Ref. [121], copyright © 2022, American Chemical Society. (b) Chemical structures of porphyrin with O-linked cationic side chains. (c) The formation processes and biological applications of O_2@PFOB@PGL NPs. Reprinted with permission from Ref. [123], copyright © 2020, American Chemical Society. (d) The formation processes of ATO/ZnPc-CA@DA. Reprinted with permission from Ref. [124], copyright © 2023 Elsevier Inc. All rights reserved.

of cyanine structures and retain their fluorescence and therapeutic effects to the greatest extent, researchers have designed a series of functional nanomaterials to meet the needs of *in vivo* applications. Wang et al. introduced carboxyl or sulfonic acid groups into the indole ring or branch of the asymmetric heptamethine cyanine to design and synthesize a series of cyanine phototheranostic reagents, and BSS-Et showed the best photophysical properties (Fig. 17a). Co-assemble BSS-Et and DSPE-PEG2000 to construct BSS-Et NPs to achieve visual ablation of tumors [111].

BAC808, which can be activated FL/PDT/PTT under acidic conditions, was selected as the phototheranostic part, the tumor-targeted DSPE-PEG-cRGD and tumor microenvironment-severable DSPE-PEG-S-S-PEG-DMMA self-assembled with BAC808 to fabricate DMMA@cRGD@BAC808 (Fig. 17b). DMMA@cRGD@BAC808 is selectively enriched within tumors and exerts its FL/PDT/PTT efficacy under acidic and high GSH conditions for imaging-guided phototherapy [112]. Different from the above strategies, Chen et al. covalently modified the PEG chain on the cyanine structure to increase its dispersion in physiological environments. The obtained amphiphilic cyanine structure was then self-assembled with other functional parts to construct multifunctional nanoparticles [113].

Compared with other types of polymer organic structures and inorganic structures, biological carriers such as albumin have better biocompatibility, excellent biodegradability, and non-immunogenicity, which are widely used to deliver drugs *in vivo* [114]. c-Met is an attractive biomarker for colorectal tumors because it is highly expressed

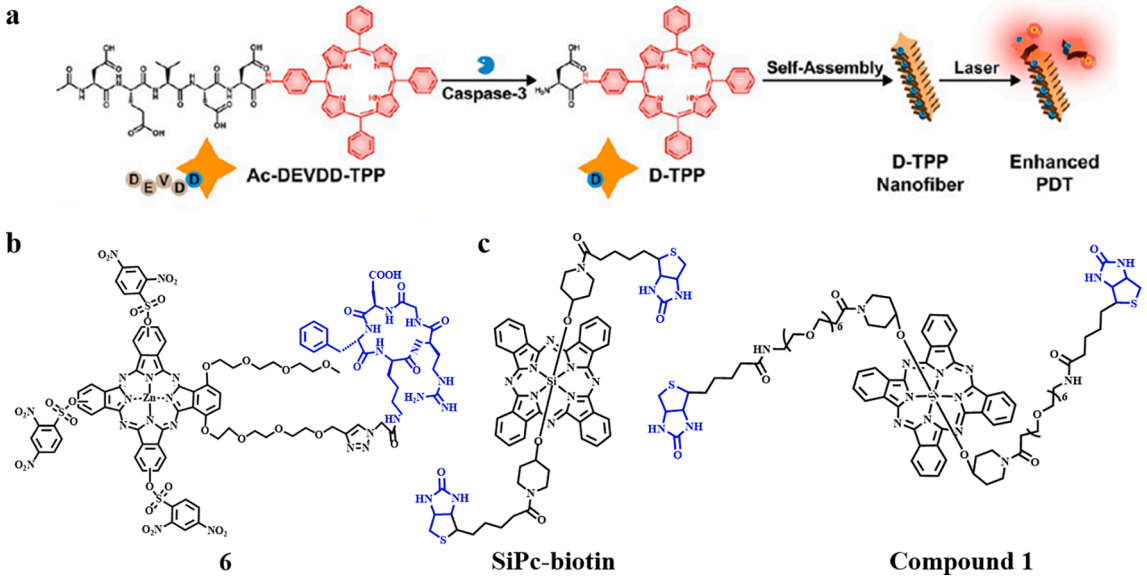

Fig. 19. (a) Chemical structure of Ac-DEVDD-TPP and its self-assembly. Reprinted with permission from Ref. [125], copyright © 2023, American Chemical Society. (b) Chemical structure of 6. (c) Chemical structures of SiPc-biotin and compound 1.

in colorectal adenomas and barely detectable in normal colon tissue [115]. Crizotinib has a favorable targeted inhibitory effect on c-Met-positive tumors. Chen et al. covalently bound crizotinib to IR808 and synthesized the Crizotinib-IR808 organic molecular structure. To increase biological safety, Crizotinib-IR808 was self-assembled with BSA to construct Crizotinib-IR808@BSA NPs to achieve tumor-specific targeted NIR II fluorescence imaging-guided phototherapy (Fig. 17c) [116].

4. Tetrapyrrole structures-based fluorescence imaging-guided theranostics for cancer therapy

Tetrapyrrole structures, they are mainly divided into two major categories in this review, porphyrins and phthalocyanines. Porphyrin is known as the "life pigment" and it is ubiquitous in nature and has strong light absorption, O_2 transport and other functions. Due to its inherent π-conjugated structure, this type of compound is endowed with unique photophysical properties [117]. Porphyrin has a strong Soret band (about 400 nm) and Q-band (500–600 nm) in the visible light region, and its absorption spectrum can be red-shifted to the NIR light region by structurally modifying different aromatic rings [118,119]. As a second-generation PS, phthalocyanine is widely used in phototherapy due to its relatively long absorption wavelength (>660 nm), high extinction coefficients ($>10^5$ L mol^{-1} cm^{-1}), and controllable photophysical and chemical properties [120]. In this section, we list the advantages, disadvantages and other characteristics of some representative structures (Table 2) and we will classify and summarize different strategies to increase their phototherapeutic effects, including overcome tumor hypoxia, tumor, sub-organelle targeting, and aggregation regulation etc.

4.1. Overcome the hypoxia enhanced PDT

The hypoxic condition of tumors limits the effectiveness of PDT, especially type II PDT, and the O_2 consumed during the PDT process aggravates the hypoxia of the tumor. Yoon's group used silicon phthalocyanine as the precursor, modified the acid-responsive lysosome targeting morpholine structure, and synthesized the PcM precursor. To increase its biocompatibility and tumor targeting, PcM was self-assembled with albumin to construct NanoPcM. Due to the intramolecular PET and aggregation-induced quenching effect, NanoPcM exhibits quenched fluorescence. In an acidic environment, the PET effect is inhibited and NanoPcM disassembles, thereby restoring its fluorescence (Fig. 18a). After testing, it was found that NanoPcM is an efficient type I phototheranostic reagent, which is beneficial to the treatment of tumors in hypoxic environments [121]. The low solubility and aggregation-induced ROS quenching properties of porphyrins make them unsuitable for PDT treatment of hypoxic tumors. Song et al. designed and synthesized water-soluble porphyrins with O-linked cationic side chains, which have better water solubility, photostability, and type I and type II photophysical properties to overcome tumor hypoxia (Fig. 18b) [122].

Unlike porphyrin single-molecule modifications to improve their solubility, Dai and co-workers dispersed perfluorooctyl bromide (PFOB) liquid into lipid-modified porphyrin (PGL) nanoparticles through ultrasonic dispersion. Then O_2 was loaded to construct O_2@PFOB@PGL NPs (Fig. 18c). This nanomaterial has a porphyrin loading rate as high as 38.5 %, which ensures its fluorescence and phototherapy properties. Through the release of O_2, it increases the production of $^1O_2$, relieves tumor hypoxia, and promotes the downregulation of COX-2 expression, which is beneficial to the elimination of tumors and the inhibition of tumor metastasis [123]. Cationic and anionic zinc phthalocyanines are self-assembled into ZnPc-CA nanomaterials through electrostatic reaction, and then atovaquone (ATO) is loaded and polydopamine is coated on the surface of the nanomaterials to obtain ATO/ZnPc-CA@DA (Fig. 18d). ATO/ZnPc-CA@DA shows excellent stability in normal tissues. In acidic condition, it will trigger the dissociation of nanomaterials, resulting in fluorescence enhancement and ROS increase [124].

4.2. Tumor or/and subcellular organelle targeting enhanced PDT

Unlike cyanine, porphyrin and phthalocyanine derivatives do not have the natural tumor targeting properties. To increase their tumor targeting properties, further structural modification or the assembly of nanomaterials is required. Liang et al. covalently modified the peptide chain on the porphyrin structure and synthesized the Ac-Asp-Glu-Val-Asp-Asp-TPP (Ac-DEVDD-TPP) porphyrin structure. After laser irradiation, this structure causes cell apoptosis and promotes the expression of cysteinyl aspartate specific proteinase 3 (Casp3), which is conducive to the cleavage of the Ac-DEVDD-TPP structure to produce D-TPP (Fig. 19a). The released D-TPP further self-assembles into D-TPP porphyrin nanofibers for enhanced tumor treatment [125].

Folic acid, also known as vitamin B9, is a nutrient required by all living cells for nucleotide synthesis and cell growth. Folate works by specifically targeting the folate receptor. Folate receptors are highly expressed in epithelial tissues of various tumors compared with normal tissues, and therefore can be used as tumor-targeting ligands [126]. Constructing porphyrin nanomaterials by modifying folic acid is beneficial to enhance tumor targeting [127].

Integrins are the major extracellular matrix (ECM) receptors. Integrin αvβ3 is highly expressed in endothelial cells and pericytes, and it can bind to ECM containing the arginine-glycine-aspartate (RGD). Therefore, drug delivery systems based on RGD molecules are capable of targeted transport and release at the tumor site [128,129]. Huang and co-workers constructed compound 6b, which is highly selective for $\alpha v\beta 3^+$ tumor cells, by axially substituting cyclic arginine-glycine-aspartic acid (cRGD) on silicon (IV) phthalocyanine. 6b can be entered tumor cells through integrin-mediated endocytosis to achieve its tumor-killing effect [130]. Ng' group used three 2,4-dinitrobenzene sulfonic acid (DNBS) groups and a cRGD structure to graft onto zinc(II) phthalocyanine to synthesize new compound 6 (Fig. 19b). The presence of DNBS in compound 6 leads to the quenching of its fluorescence and PDT. In the presence of GSH, DNBS is cleaved to release fluorescence and

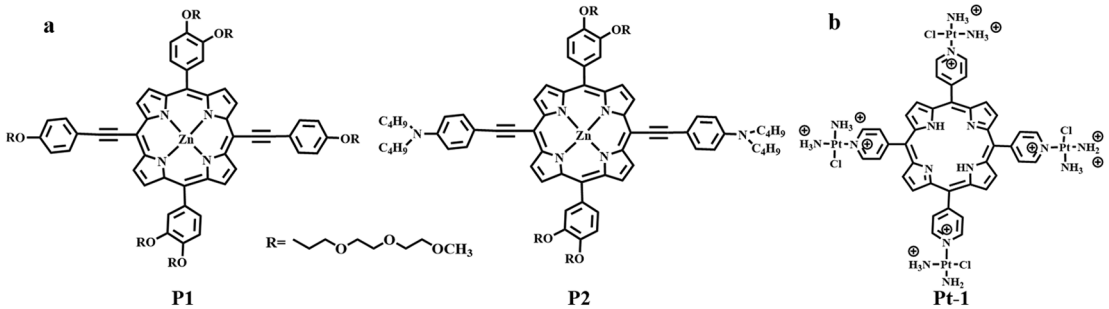

Fig. 20. Chemical structures of P1, P2 (a) and Pt-1(b).

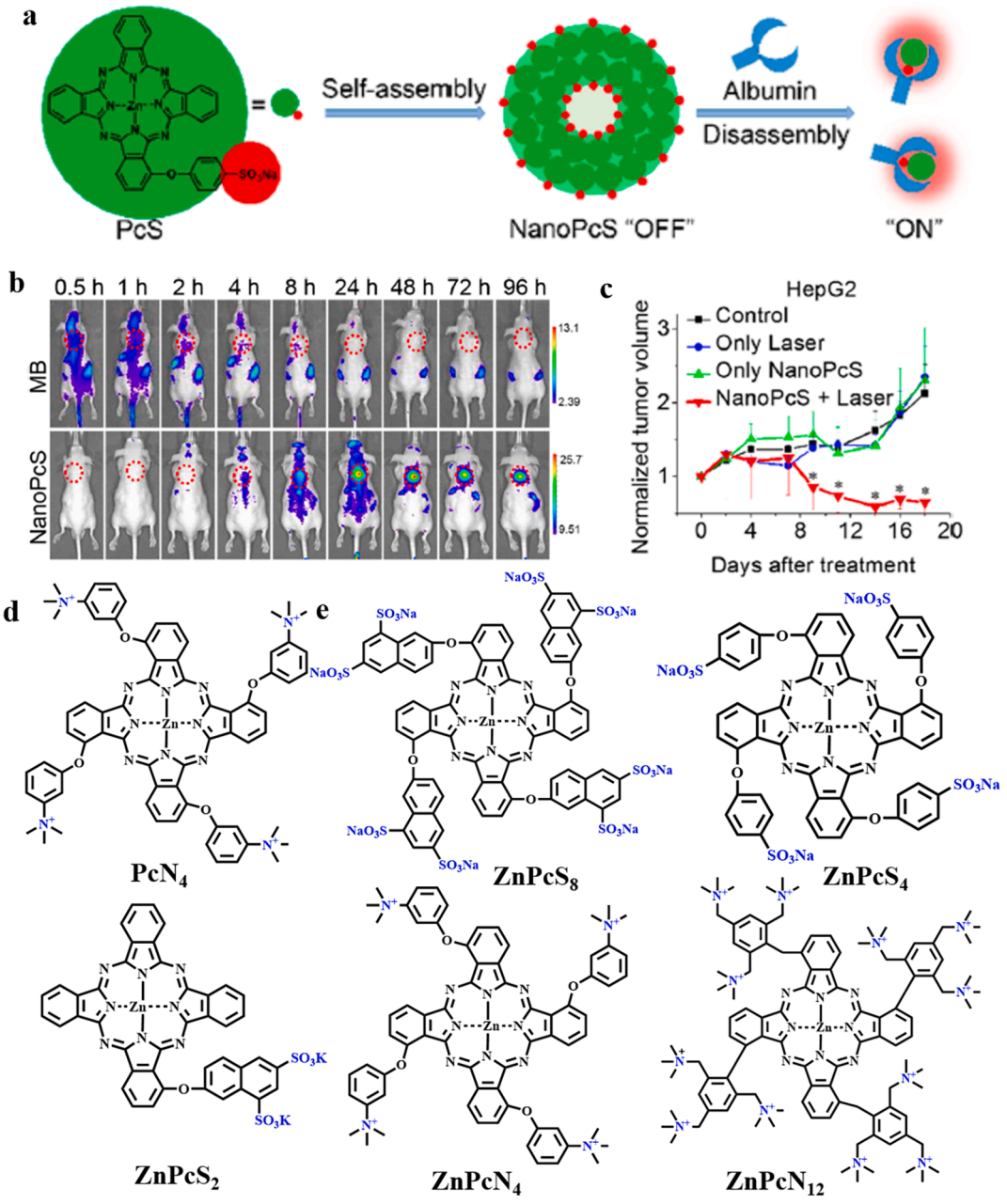

Fig. 21. (a) Chemical structure of PcS and its self-assembly. (b) *In vivo* fluorescence images of HepG2 tumor-bearing mice after post-injection of MB and NanoPcS. (c) Tumor growth of mice after various treatments. Reprinted with permission from Ref. [147], copyright © 2019, American Chemical Society. Chemical structures of PcN_4 (d), $ZnPcS_8$, $ZnPcS_4$, $ZnPcS_2$, $ZnPcN_4$ and $ZnPcN_{12}$ (e).

restore $^1O_2$ production. The RGD-like peptide sequence can enhance its localization to tumor cells, thereby achieving recognition and killing of tumor cells [131].

Biotin, also known as vitamin H, is essential for cell growth. In view of the rapid proliferation of tumors, tumor cells require more biotin than normal cells. Therefore, biotin receptors are highly expressed in tumor cells, which can serve as tumor markers [132].

Lin et al. constructed SiPc-biotin and compound 1 organic molecules by modifying biotin on silicon phthalocyanine (Fig. 19c). Compound 1 has added polyethylene glycol (PEG) chains, so its hydrophilicity and water solubility are higher than that of SiPc-biotin. Both compounds achieve the selective recognition and accumulation of biotin-positive tumor cells, achieving the effect of tumor elimination [133,134].

In terms of molecular structure modification, to further improve the selective enrichment ability of organic molecules in tumor cells and the targeting ability of subcellular organelles, lipophilic groups were introduced into the phthalocyanine skeleton. This is due to the fact that lipophilic groups are preferentially transported by lipoproteins and directly taken up by tumor cells [135]. Compounds based on positive charges are more likely to be targeted on mitochondria. Positively charged rhodamine is introduced into the silicon phthalocyanine parent to achieve targeted enhanced fluorescence imaging guided PDT [136].

4.3. *Self-assembly to construct nanomaterials for enhanced PDT*

Most porphyrins and phthalocyanine structures have hydrophobic properties, so they often aggregate in physiological environments, resulting in poor tumor targeting and poor therapeutic effects. In order to solve the above issues, researchers have developed a series of strategies to enhance its water solubility, increase targeting ability and

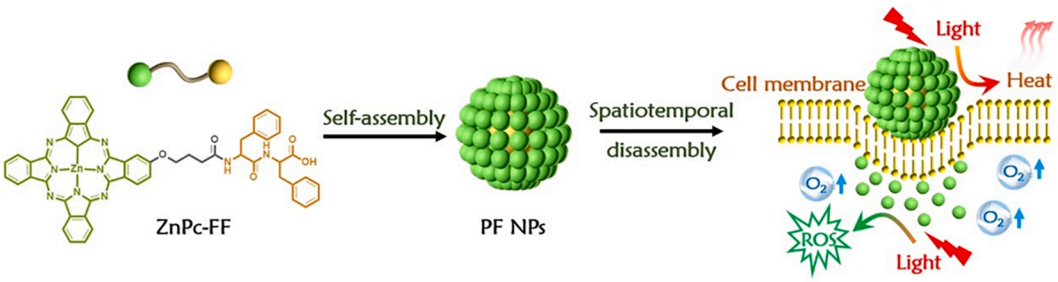

Fig. 22. Chemical structure of ZnPc-FF and its self-assembly. The spatiotemporally coupled photoactivity of PF self-assemblies is also presented. Reprinted with permission from Ref. [156], copyright © 2019 Wiley-VCH Verlag GmbH & Co. KGaA, Weinheim.

therapeutic effect: self-assembly of phototheranostic agents after structural modification [137], self-assembly of phototheranostic agents with polymer [138–140], as well as the self-assembly of phototheranostic agents with metal–organic frameworks or metal nanomaterials, etc [141–143]. Visualized phototherapy of tumors can be achieved by constructing nanoaggregates, nanocomposites, etc.

Dong et al. synthesized two new *meso*-A2B2-porphyrins (P1 and P2) with symmetric phenylacetylene groups by introducing amphiphilic triethylene glycol into the porphyrin skeleton (Fig. 20a). The obtained P1 and P2 prepared corresponding hydrophilic nanoparticles through solvent exchange. These self-assembled nanoparticles exhibit a red shift in absorption, better biocompatibility, and higher phototoxicity [137]. Zheng's group first synthesized the porphyrin-cisplatin organic compound molecule (Pt-1, Fig. 20b), and then self-assembled Pt-1 with a ROS-sensitive polymer to construct the nanomaterial NP@Pt-1 to achieve the combination of phototherapy and chemotherapy [139]. Dai et al. self-assembled amphiphilic porphyrin-grafted lipid (PGL) and small-sized iron oxide to construct ultra-small-sized Fe_3O_4@PGL nanoparticles (~10 nm). This self-assembly method ensures the high loading efficiency of porphyrin organic compounds. After laser irradiation, it can not only trigger fluorescence and generate sufficient ROS for PDT, but also trigger ferroptosis by regulating the tumor microenvironment [141].

4.4. Protein/nucleic acid regulate aggregation state for enhanced PDT

Albumin is a biomarker for a variety of diseases and has recently been used as a drug delivery carrier. Albumin is very abundant in plasma, and changes in albumin levels in blood are related to the development of various diseases, such as liver damage [144]. Hydrophobic organic anions or molecular structures can enter the hydrophobic cavity of albumin. Therefore, albumin can be used to capture hydrophobic organic molecules or their nanoaggregates [145,146].

Taking advantage of this property of albumin, Yoon's team synthesized an amphiphilic 4-sulfophenoxy mono-α-substituted zinc (II) phthalocyanine structure (PcS). PcS self-assembles in aqueous solution to form nanostructured NanoPcS, which shows quenched fluorescence. When NanoPcS enters the blood, it will be recognized by the abundant albumin, form an albumin-PcS nanocomplex, and restore its fluorescence (Fig. 21a). Whole-body fluorescence imaging results suggested that after NanoPcS was injected into the tumor-bearing mice through the tail vein, it gradually accumulated in the tumor site and showed a "turn on" fluorescence signal (Fig. 21b). After exposure to light, the growth of HepG2 tumors was significantly inhibited (Fig. 21c) [147]. Using the same principle, this group constructed another water-soluble phthalocyanine molecule named PcN_4. The detailed structure is shown in the Fig. 21d. When PcN_4 enters the blood, it can construct a nanocomplex with albumin to restore the fluorescence, and then the nanocomplex can be used in combination with the hypoxia-activated prodrug AQ4N to enhance the PDT effect [148].

To further explore the binding ability of phthalocyanine structures with different charges to albumin monomers or dimers, this group designed and synthesized five zinc phthalocyanine molecules, namely $ZnPcS_8$, $ZnPcS_4$, $ZnPcS_2$, $ZnPcN_4$ and $ZnPcN_{12}$ (Fig. 21e). It was found that two positively charged phthalocyanine compounds can specifically bind to albumin dimers, while three negatively charged phthalocyanines can bind to both albumin monomers and dimers. After binding to albumin, it promotes the generation of ROS [149].

Table 3
Summary of fluorescence, therapeutic modalities, advantages and disadvantages of representative PSs among BODIPY structures-based molecular or nanomaterials.

Photosensitizer	Fl.	Ther. Mod.	Advantages	Disadvantages	Ref.
iodine disubstituted BODIPY modified erlotinib	NIR I	PDT (type II)	high molar absorption coefficient and tumor inhibition rate; EGFR-positive tumors target	O_2-dependent PDT	[162]
covalently connected cationic rhodamine and diiodo-substituted BODIPY	NIR I	PDT (type II)	high tumor targeting; increased light-harvesting ability; mitochondrial anchoring ability	O_2-dependent PDT; the tendency for dark toxicity	[164]
dibromo-substituted BODIPY grafted acetazolamide	NIR I	PDT (type II)	relieve hypoxia; CAIX-overexpressing tumor cells targeting; inhibit tumor angiogenesis	synthesis steps are relatively complex	[167]
thienopyrrole-fused BODIPY	NIR I	PDT (type II)	increased extinction coefficient and Φ_Δ	relatively low fluorescence penetration depth	[170]
multipolar triphenylamine-BODIPY	two photon	PDT (type I and II)	higher Φ_Δ and better Φ_f; enhanced imaging depth	relatively poor water solubility	[173]
glycosylated Aza-BODIPY self-assembled into nanofibers	NIR I	PDT (type I)	tumor-targeted ability; anti-hypoxia; long retention; cell membrane damage	relatively low fluorescence penetration depth	[51]
BODIPY modified with trifluoromethyl and CPT	NIR I	PTT	improved PCE; enhanced biocompatibility	synthesis steps are relatively complex	[178]
morpholine modified aza-BODIPY based nanoparticles	NIR I	PDT & PTT	increased water solubility; high cytotoxicity for tumor cells; rapid metabolic kinetics	relatively poor tumor targeting ability	[181]
rigid coplanar aza-BODIPY modified tetrastyrene	NIR II	PDT & PTT	enhanced imaging penetration depth; improved PCE and ROS generation;	unable to inhibit tumor metastasis and recurrence	[186]

Fl., fluorescence; Ther. Mod., therapeutic modalities; Ref., reference; EGFR, epidermal growth factor receptor; CAIX, carbonic anhydrase IX; Φ_Δ, singlet oxygen quantum yield; Φ_f, fluorescence quantum yield; CPT, camptothecin; PCE, photothermal conversion efficiency.

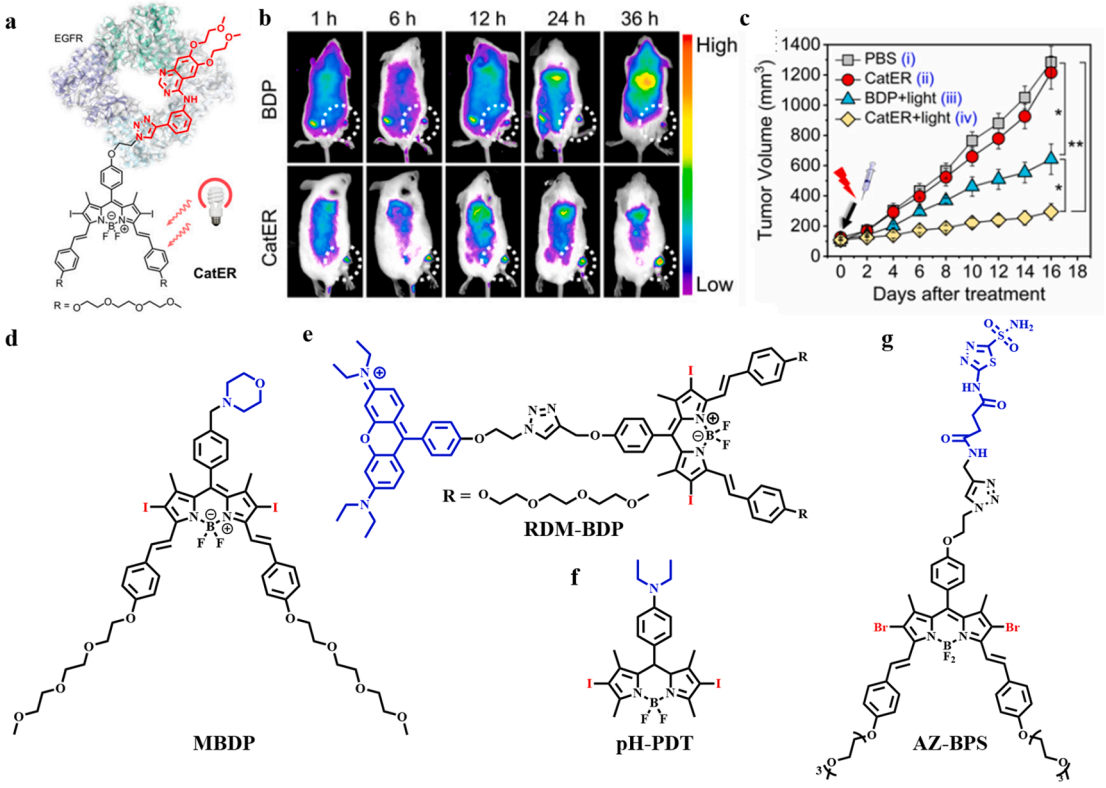

Fig. 23. (a) Chemical structure of CatER. (b) *In vivo* whole-body fluorescence imaging of tumor-bearing mice after injection of BDP or CatER. (c) Tumor growth of mice after various treatments. Reprinted with permission from Ref. [162] (a-c), Copyright © 2022 the Author(s). Published by PNAS. Distributed under CC BY-NC-ND 4.0 DEED. Chemical structure of MBDP (d), RDM-BDP (e), pH-BODIPY (f), and AZ-BPS (g).

4.5. Other methods for enhanced PDT

Combining the donor–acceptor (D-A) into the same nanoparticle utilizes energy transfer to achieve high $^1O_2$ generation and strong fluorescence emission. Tang et al. used 5,10,15,20-tetraphenylphorphyrin (H2TPP) as acceptor and poly[N,N'-bis(4-butylpheny)-N,N'-bis(phenyl) benzidine] (ADS254BE) as donor to construct ADS254BE/H2TPP NPs nanomaterials. The fluorescence emission of ADS254BE/H2TPP NPs is red-shifted to about 650 nm and has a high $^1O_2$ yield [150].

Phototheranostic agents activated by the tumor environment can significantly reduce background fluorescence as well as the side effects of phototherapy on normal tissues. LDH-$ZnPcS_8$ is constructed by electrostatic interaction between negatively charged octasulfonate-modified zinc phthalocyanine ($ZnPcS_8$) and cationic hydroxide layers of layered double hydroxide (LDH). Under neutral conditions, it exhibits quenched fluorescence and $^1O_2$ generation. The fluorescence and the photoactivity can be restored under slightly acidic tumor environment [151]. This group also constructed nanomaterials (PcS-MA) by co-assembly of zinc phthalocyanine and the anti-cancer drug mitoxantrone (MA). PcS-MA exhibited a quenched state of fluorescence and $^1O_2$ production. After reacting with nucleic acids, it is partially disassembled and the phototheranostic property is restored [152].

4.6. Phthalocyanine nanomaterials for combined PDT and PTT

Phthalocyanines are more commonly used for PDT against tumors, while organic molecules and nanostructures used for PTT are relatively rare. Some nanomaterials can have both photodynamic and photothermal properties through structural modification or changes in assembly ways [153,154]. Strategy 1: Construct nanocomposite materials with metals to improve photodynamic effects and PCE. For example, Yang et al. modified a new manganese phthalocyanine ($MnPcE_4$) PS with strong NIR absorption with Bi to construct a Bi/MnPcE4 nanocomposite for fluorescence imaging-guided photodynamic/photothermal synergistic therapy to overcome tumor hypoxia [155]. Strategy 2: Space-time coupling of photoactivity conversion to achieve switching of treatment methods. Yan's group designed and synthesized a molecular structure ZnPc-PF based on phthalocyanine and peptides. ZnPc-PF self-assembled into PF nanoparticles (PF NPs) in aqueous solution. PF NPs exhibit excellent photothermal properties. Interestingly, when PF NPs interacts with cell membranes, photoactivity conversion occurs, PF NPs exhibits photodynamic and fluorescent properties (Fig. 22). In other words, PF NPs can achieve two different photoactivities before and after transmembrane [156].

5. BODIPY-based fluorescence imaging-guided theranostics for cancer therapy

BODIPY dyes have high fluorescence stability, strong molar extinction coefficient, high Φ_f, so it is often used in fluorescent dyes [157,158]. A significant defect of the BODPIY core is that the excitation region is about 500 nm, which is far away from the NIR region. However, the structure of BODIPY is controllable. Through structural modification, it can promote the red shift of absorption and fluorescence emission to the NIR region, such as fused ring expansion via introducing the thiophene or furan moiety, and replacing the meso carbon atoms with nitrogen atoms (aza-BODIPY), etc [159]. This type of BODIPY compounds with improved structure are not only used for fluorescent dyes, but also developed as PSs. Section 5 summarizes the molecular structure improvements of BODIPY and strategies for constructing nanomaterials to enhance their photophysical and chemical properties. Simultaneously, we also list the advantages, disadvantages and other characteristics of some representative structures to better elucidate the properties of BODIPY-based molecules or nanomaterials (Table 3).

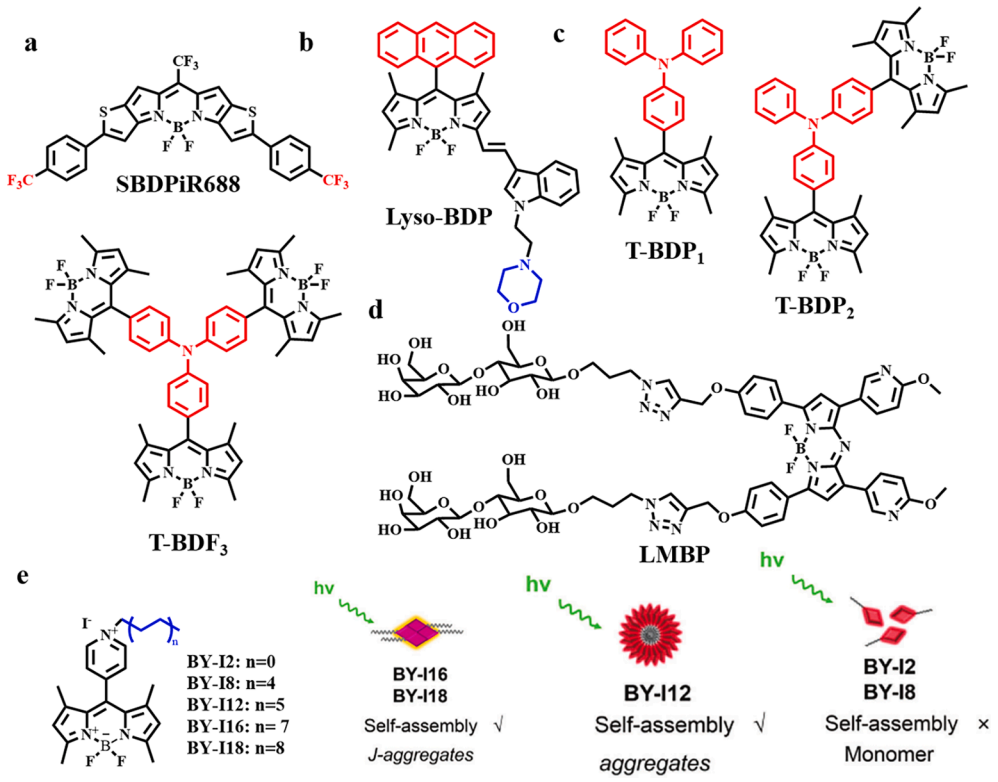

Fig. 24. Chemical structure of SBDPiR688 (a), Lyso-BDP (b), and (c) T-BDPn (n = 1, 2, 3). (d) Chemical structure of LMBP. (e) Chemical structure of BY-I2, BY-I8, BY-I12, BY-I16, BY-I18 and their nanoform. Reprinted with permission from Ref. [176], copyright © 2023 Wiley-VCH GmbH.

5.1. Heavy atoms enhanced PDT

The BODIPY core structure has a low possibility of reaching the triplet state through ISC after illumination. Therefore, its ISC capability can be increased by introducing heavy atoms (such as I, Br, etc.) or complexing with transition metals, so that the high fluorescence emission and low triplet transitions are converted into high triplet transitions and appropriate fluorescence emission, thereby increasing the quantum yield of $^1O_2$. The 2 and 6 positions of the BODIPY core are prone to electrophilic aromatic substitution of I or Br. Therefore, heavy atoms can be modified at this position to increase the ability of ISC and achieve photophysical property conversion [160].

In addition to modifying heavy atoms to increase the yield of $^1O_2$, the effect of phototheranostics can also be further enhanced by increasing tumor and subcellular organelle targeting, constructing tumor microenvironment activation structures, and overcoming the limitations of the tumor hypoxia.

Epidermal growth factor receptor (EGFR) is highly expressed in a variety of tumors, such as lung cancer, head and neck cancer, and ovarian cancer [161]. Kim and co-workers designed and synthesized a new CatER that can selectively target EGFR, which consists of two parts: iodine disubstituted BODIPY and the FDA-approved tyrosine kinase inhibitor erlotinib (target and inhibit EGFR). The specific chemical structure is shown in Fig. 23a. CatER has significant absorption at 600–700 nm, and the molar absorption coefficient at 660 nm reaches 65,042 $M^{-1} \times cm^{-1}$. Under 660 nm laser irradiation, the center of the fluorescence emission spectrum moves to 702 nm, and the absolute Φ_f is 0.06. CatER selectively targets EGFR-positive tumors, using $EGFR^+$ 4 T1 tumor-bearing Balb/c mice as a model, *in vivo* fluorescence imaging indicated that compared with BDP (molecules without erlotinib modification), CatER showed excellent tumor-targeted imaging capabilities (Fig. 23b). After irradiation with 660 nm laser for 20 min, the tumor inhibition rate of CatER was as high as 77.1 %, while the tumor inhibition rate of BDP was about 46 %, indicating that adding EGFR targeting group was beneficial to phototheranostic agents to improve the selective targeting of tumors and enhance the therapeutic effect (Fig. 23c) [162]. To increase the lysosome targeting ability of phototheranostic agent, Peng et al. modified the lysosome-targeting morpholine structure onto the double-iodinated BODIPY structure and named it MBDP to achieve lysosome-targeted phototheranostics (Fig. 23d). After illumination, the IC_{50} value of MBDP is as low as 0.2 μM, which is significantly lower than the traditional Ce6 photosensitizer (1.39 μM) [163]. Subsequently, this group covalently connected cationic rhodamine and diiodo-substituted BODIPY (BDP) to prepare RDM-BDP, based on the Förster resonance energy transfer (FRET) mechanism (the

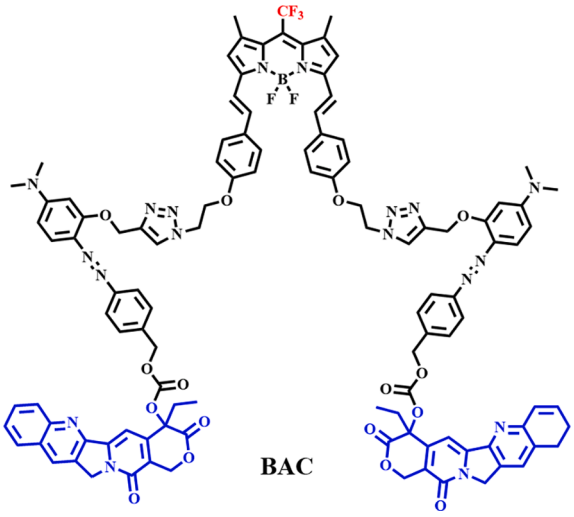

Fig. 25. Chemical structure of BAC.

rhodamine part serves as the donor, and the BDP part serves as the acceptor) to achieve tumor-specific recognition and efficient fluorescence-imaging guided phototherapy (Fig. 23e). After intravenous injection of RDM-BDP, the tumor site showed significant fluorescence enhancement, and the signal ratio to adjacent tissue was as high as 12.5. Benefiting from the FRET effect, the absorption band of RDM-BDP is broader, which increases the light capture ability and is beneficial to the produce of $^1O_2$. The cationic rhodamine structure not only increases the tumor targeting ability, but also enhances the mitochondrial targeting effect, showing a 13-fold enhanced cellular uptake ability [164].

To ensure the PDT effect of phototheranostic agent can be activated under the specific environment of the tumor, Yi's team constructed a pH-responsive BODIPY structure, named pH-BODIPY (Fig. 22f). The highly sensitive pH range of pH-BODIPY is 5.5–3.0, and under acidic conditions, the Φ_Δ increases from 0.24 to 0.45 [165].

The hypoxic microenvironment of tumors limits the effectiveness of PDT, especially the production of $^1O_2$. What's worse, PDT treatment aggravates tumor hypoxia, which may lead to cancer recurrence by activating various angiogenic factors. Carbonic anhydrase IX (CAIX) can regulate intracellular and extracellular pH and promote tumor survival and invasion in hypoxic environments. CAIX is a marker for aggressive breast cancer such as MDAMB-231 cell [166].

AZ-BPS, a compound modified with acetazolamide (AZ) on the structure of dibromo-substituted BODIPY was reported by Kim's group (Fig. 23g). AZ-BPS can relieve hypoxia and eliminate tumors through anti-angiogenesis and PDT. AZ part can not only target CAIX-overexpressing tumor cells, but also inhibit CAIX; the double-bromo-substituted BODIPY can be used as the fluorescence imaging and the PDT. Therefore, AZ-BPS can simultaneously achieve imaging-guided phototherapy and inhibit tumor angiogenesis to alleviate tumor hypoxia [167]. Different from the above strategy, Peng et al. reported in 2020 that nanomaterials were constructed by combining diiodo-substituted BODIPY with peroxidase liposomes. With the help of peroxidase liposomes, this nanoparticle can catalyze excess H_2O_2 in tumors to generate O_2 to enhance $^1O_2$ yield and alleviate tumor hypoxia [168].

5.2. *Heavy atom-free effect enhanced PDT*

The introduction of heavy atoms into the molecular structure can significantly increase its singlet oxygen quantum yield, but it may also cause increased dark toxicity and metabolism-related problems *in vivo* [169]. BODIPY themselves have certain photodynamic properties. By introducing a glycosylated styrene group at the C-3 site, they have better PDT properties than other sites. You et al. found that thienopyrrole-fused BODIPY (SBDPiR690) dye can produce $^1O_2$ and fluorescence. To this end, the group prepared a series of SBDPiR analogues with electron-withdrawing groups in the *para*-position of the phenyl group to increase highest occupied molecular orbitals (HOMOs)-lowest unoccupied molecular orbitals (LUMOs) energy gap and $^1O_2$ production. Among them, SBDPiR688, which introduces CF_3, has high extinction coefficient (211000 M^{-1} cm^{-1}) and balanced decay (Fig. 24a) [170].

The spin–orbit charge transfer ISC (SOCT-ISC) mechanism was proposed by professor Willigen. He connected naphthalene and acridine through covalent bonds to form a D-A binary compound with an orthogonal configuration [171]. After light excitation, the charge transfer process occurs within the molecules. After the process of charge separation and charge recombination, ISC is realized and a triplet state is generated. Based on this theory, Zhao et al. designed and synthesized the lysosome-targeted BODIPY PS Lyso-BDP (Fig. 24b). The anthracene group and BODIPY were combined to form a D-A binary compound. Lyso-BDP has 62 % high $^1O_2$ quantum yield in DCM, and the IC_{50} for 4 T1 cells is 2.5 μM [172]. In the same year, as shown in Fig. 24c, Qian and co-workers synthesized a series of multipolar triphenylamine-BODIPY photosensitizers T-BDPn (n = 1, 2, 3). Compared with the D-A configuration of T-BDP1, multipolar T-BDP3 dendrimers with higher $^1O_2$ efficiency (44 %) and betterΦ_f (7.45 %). Through theoretical calculations and femtosecond transient absorption spectroscopy experiments, it was found that the multipolar T-BDP3 dendrimers can produce more triplet states, which can further increase the SOCT-ISC process. What's more, T-BDP3 can produce $O_2^{\bullet-}$ after being illuminated at 800 nm. Overall, T-BDP3 can be used for two-photon imaging-guided type I and type II synergistic phototherapy [173].

J-aggregates will have a red shift in absorption relative to their monomers [174]. Phototheranostic agents in J-aggregates exhibit slight

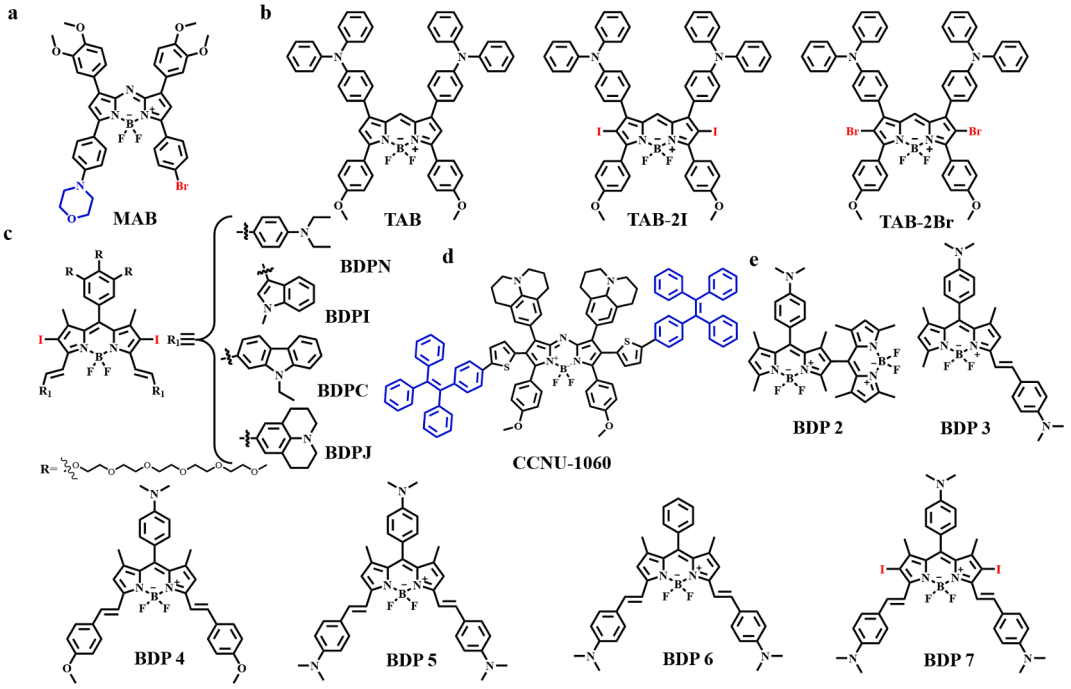

Fig. 26. Chemical structure of MAB (a), (b) TAB, TAB-I, and TAB-Br; (c) BDPN, BDPI, BDPC, and BDPJ; (d) CCNU-1060; (e) BDP 2 – 7.

Table 4
Summary of fluorescence, therapeutic modalities, advantages and disadvantages of representative PSs among AIEgens-based molecular or nanomaterials.

Photosensitizer	Fl.	Ther. Mod.	Advantages	Disadvantages	Ref.
tetrastyrene derivative combined with $^1O_2$-cleavable AA and cRGD	NIR I	PDT (type II)	high tumor targeting; monitoring of $^1O_2$ generation; early evaluation of the therapeutic effect	synthesis steps are relatively complex; no *in vivo* applications	[192]
alkoxyl-branched TPE modified with Br	NIR I	PDT (type I and II)	membrane staining; efficient ROS generation	relatively poor *in vivo* application	[196]
N,N-dimethyl-substituted TPE modified with 4-vinylpyridine	NIR II	PDT (type I)	relieve hypoxia; cancerous mitochondria-targeting; hybrid apoptosis and ferroptosis	unable to inhibit tumor metastasis and recurrence	[202]
TPA skeleton modified with pyridine and biotin	NIR I	PDT (type I and II)	large stokes shift; tumor cells and mitochondrial targeting; sufficient ROS production	relatively low fluorescence penetration depth	[207]
TPA skeleton modified with quinolinium salt	NIR I	PDT (type I)	time-dependent subcellular organelles target; excellent type I ROS generation	relatively low fluorescence penetration depth	[208]
TPA combined with thiophene and benzothiazole 2-acetonitrile	NIR I	PDT (type I and II)	lipid droplets detection; high bioactivity and stability; enhanced ROS generation	relatively poor water solubility	[213]
5,5′-(6,7-diphenyl-[1,2,5]thiadiazolo[3,4–g]quinoxaline-4,9-diyl)bis(4-hexyl-N,N-bis(4-methoxyphenyl)thiophen-2-amine)	NIR II	PTT	increased fluorescence penetration depth and control of PCE; enhanced photostability and tumor targeting	the construction of nanomaterials is more complicated	[222]
6, 7-diphenyl-[1,2,5]thiadiazolo[3,4g]quinoxaline as the acceptor, thiophene as the π bridge, phenothiazine serves as the acceptor, and a triphenylamine rotor donor is added to the phenothiazine	NIR II	PTT	highest PCE (73.32 %); increased fluorescence penetration depth; noticeable therapeutic efficiency and biocompatibility	relatively poor water solubility; complex synthesis steps	[223]

Fl., fluorescence; Ther. Mod., therapeutic modalities; Ref., reference; AA, aminoacrylate; cRGD, cyclic arginine-glycine-aspartic acid; TPE, tetraphenylethylene; TPA, triphenylamine; PCE, photothermal conversion efficiency.

overlap of HOMOs and LUMOs, which provides advantages for enhancing ISC and photochemical reactions by reducing Δ_{EST} [175]. Xing et al. synthesized a glycosylated Aza-BODIPY compound (LMBP) that can selectively enter liver cells and assemble into J-aggregate nanovesicles in situ and then further self-assemble into J-aggregate nanofibers, which can be used for cell membrane disruption and type I PDT (Fig. 24d and 24e). In vivo fluorescence imaging results demonstrated that LMBP owned tumor-targeted ability (Fig. 24f). After laser irradiation, the tumors were almost eliminated in LMBP group (Fig. 24g) [51]. Yoon's group synthesized a series of BODIPY compounds by adjusting the length of the tail alkyl chain. Their self-assembly performance and PDT efficiency are highly correlated with the length of the tail alkyl chain. The obtained self-assembled J-aggregates BY-I16 and BY-I18 exhibited excellent type I and type II PDT properties (Fig. 24h) [176].

5.3. *BODIPY-based nanoparticles for PTT*

PTT is a process that converts light energy into heat, causing localized hyperthermia to cause tumor cell death. The hypoxic microenvironment of the tumor has no significant impact on the efficacy, which is one of its advantages in the treatment of tumors, especially solid tumors. Previous studies found that introducing a trifluoromethyl ($-CF_3$) barrier-free rotor into the middle position of the BODPIY scaffold resulted in high PCE [177]. Inspired by this, Lin and co-workers also introduced a $-CF_3$ barrier-free rotor to the middle position of the

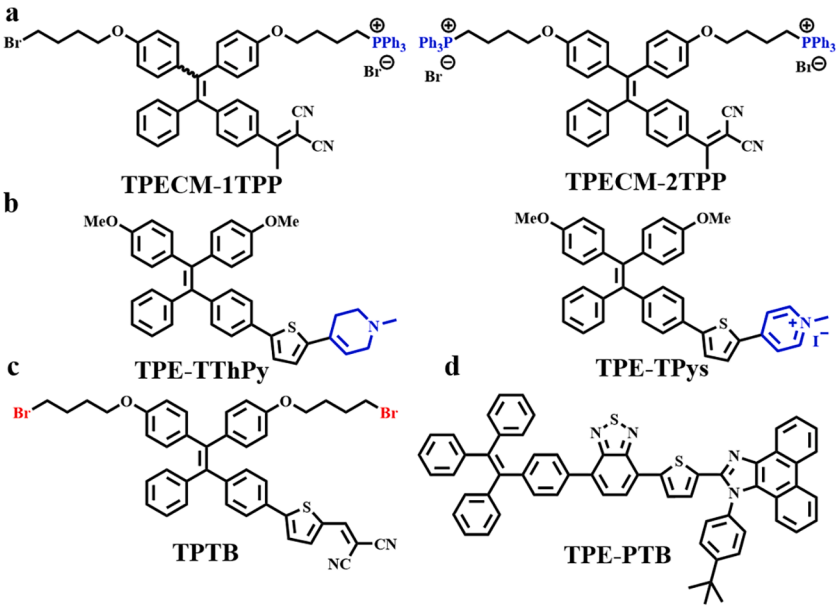

Fig. 27. Chemical structure of TPECM-1TPP, TPECM-2TPP (a), (b) TPE-TThPy, TPE-TPys; (c) TPTB; (d) TPE-PTB.

BODPIY scaffold to enhance the non-radiative decay pathway; and covalently combined it with the chemotherapy drug camptothecin (CPT) to construct a new phototheranostic agent named BAC (Fig. 25). BAC is further assembled with HSA to construct HSA@BAC nanomaterials. The PCE of HSA@BAC are calculated to be 49.0 % [178].

5.4. BODIPY-based nanomaterials for combined PDT and PTT

The combined use of PTT and PDT is a gorgeous strategy to overcome their respective shortcomings and improve anti-tumor efficacy. Because PTT can improve the O_2 supply of tumor tissues by increasing blood flow, thereby promoting the PDT effect, which in turn can eliminate heat-resistant of tumor cells to enhance PTT efficiency. Increasing the NIR absorption of molecular structures or nanomaterials by improving water solubility is one of the strategies to increase various energy dissipation ways to improve diagnostic and therapeutic effects [179,180]. Dong's team synthesized a new molecular called MAB by introducing an electron-donating morpholine structure into the aza-BODIPY skeleton to increase intramolecular electron transfer to promote its absorption red shift (Fig. 26a). To increase the solubility, MAB assembled with the amphiphilic polymer DSPE-MPEG2000 into nanoparticles, and the maximum absorption of this nanomaterial is red-shifted to 730 nm. The IC_{50} value for tumor cells is as low as 10 μg/mL under 730 nm laser irradiation [181].

While improving water solubility, heavy atoms are introduced to increase the ISC effect and simultaneously enhance the efficiency of PDT and PTT [182,183]. To verify the influence of different heavy atoms on the photophysical properties of triphenylamine-modified aza-BODIPY, Yan et al. introduced H, Br and I to the same BODIPY skeleton to get TAB, TAB-2Br and TAB-2I, respectively (Fig. 26b). To alleviate hydrophobicity, these BDOIPYs assembled with amphipathic peptide POEGMA23–PAsp20 into nanoparticles. The photophysical and chemical properties were compared. The $^1O_2$ generation ability is TAB-2I > TAB-2Br > TAB, the PCE of these three nanomaterials are 41.6 % (P-TAB), 41.5 % (P-TAB-2Br), and 42.3 % (P-TAB-2I) respectively [184]. Yin et al. introduced different groups at positions 3 and 5 of the iodine disubstituted BODIPY structure that modified the hydrophilic chain and obtained new compounds BDPN, BDPI, BDPC, and BDPJ (Fig. 26c). Each molecule has different degrees of J-aggregation due to the steric hindrance effect of the 3 and 5-position groups. Among them, BDPN NPs have suitable size, strong NIR absorption, suitable Φ_f (3.0 %), satisfactory PCE(54.9 %) and great Φ_Δ (=40.76 %) [185]. Sun and co-workers bridged flexible tetrastyrene to rigid coplanar aza-BODIPY, named CCNU-1060, and achieved fluorescence imaging-guided photodynamic and photothermal synergistic therapy by regulating three energy consumption ways (Fig. 26d) [186].

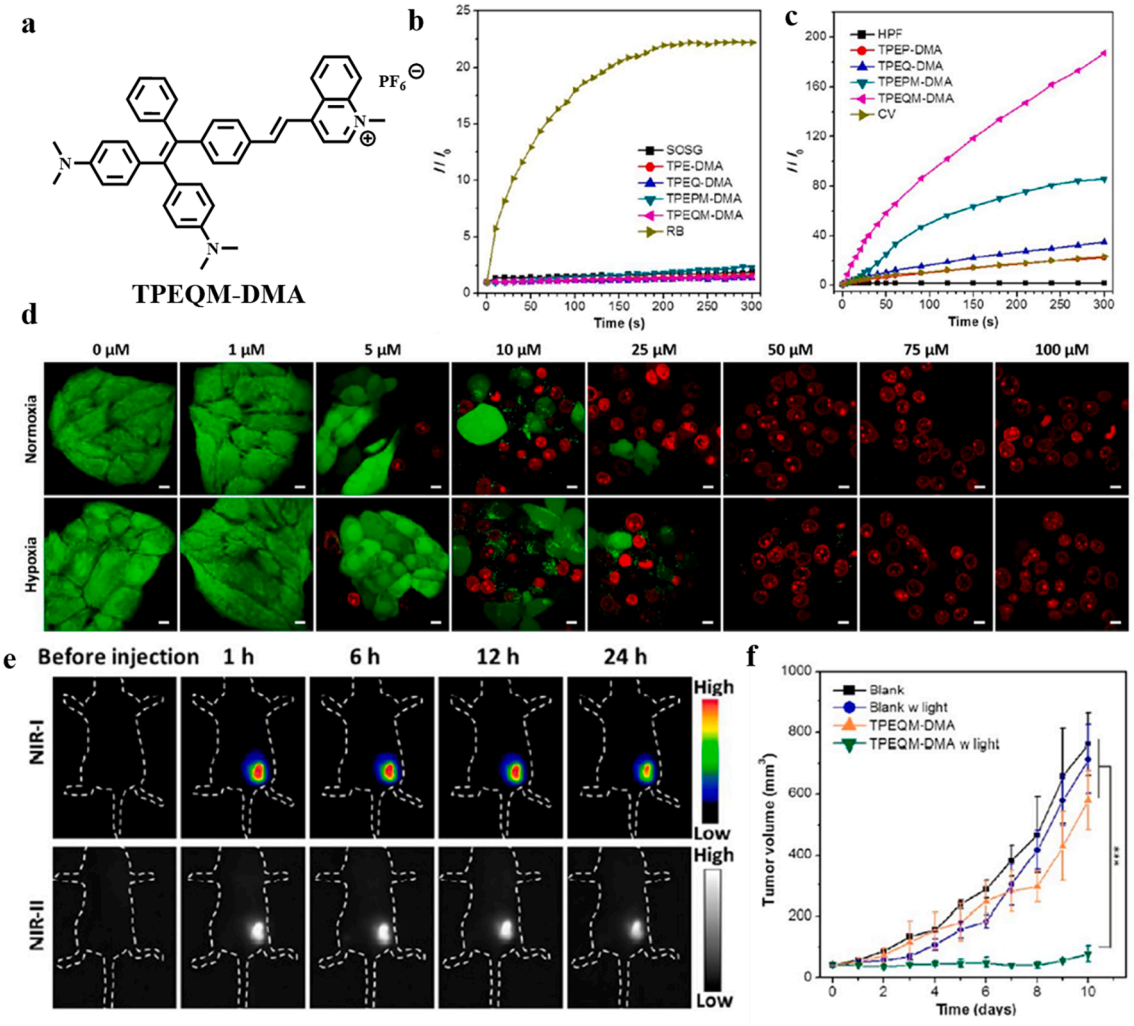

Fig. 28. (a) Chemical structure of TPEQM-DMA. (b) $^1O_2$ detection by using SOSG as probe. (c) OH• detection by using HPF as probe. (d) The live/dead cell staining assays under normoxic and hypoxic conditions. (e) *In vivo* NIR-I and NIR-II fluorescence imaging of tumor-bearing mice after injection of TPEQM-DMA. (f) Tumor growth of mice after various treatments. Reprinted with permission from Ref. [202], copyright © 2023, American Chemical Society.

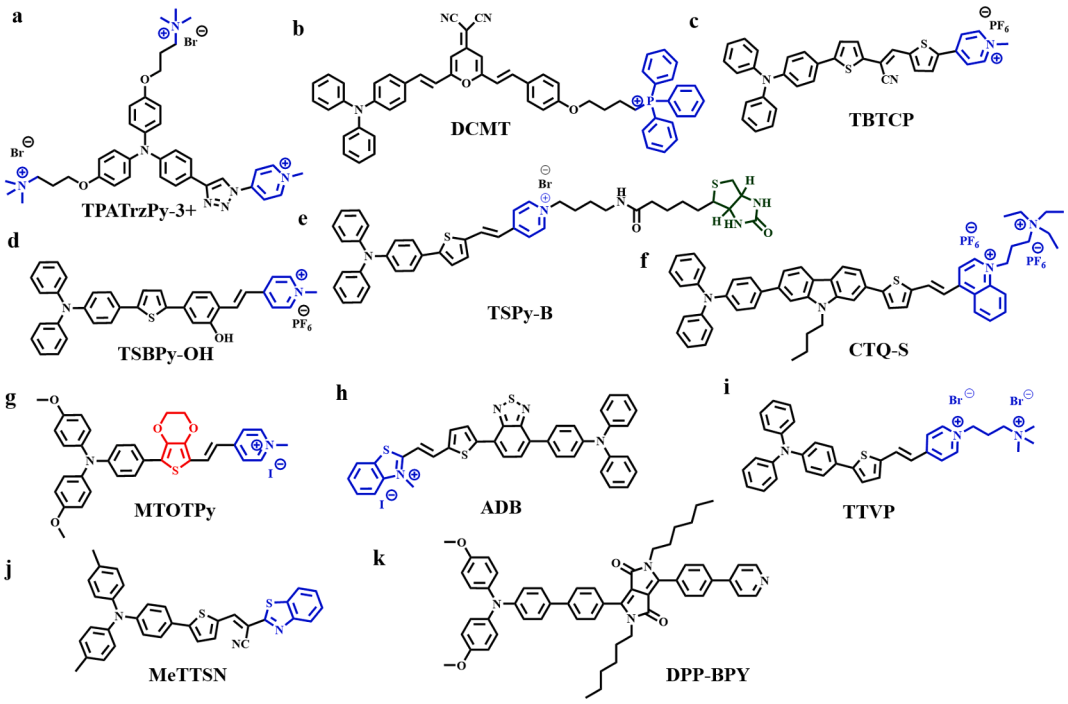

Fig. 29. Chemical structure of (a) TPATrzPy-3+; (b) DCMT; (c) TBTCP; (d) TSBPy-OH; (e) TSPy-B; (f) CTQ-S; (g) MTOTPy; (h) ADB; (i) TTVP; (j) MeTTSN; (k) DPP-BPYS.

Han et al. constructed a series of pH-responsive BODIPY analogues, named BDP 2−7 respectively. Their structures are shown in Fig. 26e. They used photoinduced electron transfer (PET), intramolecular charge transfer (ICT) and heavy atom effects to screen structure for imaging and therapeutic applications. Among them, BDP 7, which has both PET, ICT and heavy atom effect, demonstrated the most excellent imaging therapeutic effect. This may be due to the fact that the heavy atom effect increases the yield of $^1O_2$, while under acidic conditions, PET and ICT is inhibited, thereby reducing the fluorescence intensity and increasing the photothermal effect [187].

6. AIEgens −based fluorescence imaging-guided theranostics for cancer therapy

The concept of aggregation-induced emission (AIE) was first proposed by professor Tang Benzhong in 2001. It refers to the fact that organic probes do not emit fluorescence in a dilute solution state, but can emit fluorescence when in an aggregated or solid state. Structures that emit strong fluorescence emission in aggregated or solid state are called AIEgens [188,189]. Traditional phototheranostic agents such as cyanines, porphyrins, phthalocyanines, and BODIPY often exhibit quenched fluorescence and reduced ROS production capabilities in the aggregated state. This may be due to intramolecular π-π stacking, which limits *in vivo* application. Fortunately, the inherent twisted configuration and abundant free molecular rotators of AIEgens endow them with the ability to generate photothermal and ROS. At the same time, their large Stokes shift and excellent photostability promote their wide application in imaging, diagnosis and treatment. This section mainly introduces the design of classic AIEgens organic molecular structures and their aggregates and nanocomposites, the strategy of enhanced their fluorescence imaging-guided PDT\PTT or PDT combined with PTT. Also, the advantages, disadvantages and other characteristics of some representative structures based on the AIEgens were summarized (Table 4).

6.1. Tetraphenylethylene-based phototheranostic agents for PDT

The reason for the fluorescence quenching of AIE molecules in the dilute state may be that the rotation and vibration consume the absorbed energy, while in the aggregation state, the restriction of intramolecular motion (RIM) includes the restriction of intramolecular rotation (RIR) and restriction of intramolecular vibration (RIV) are considered to be the most commonly used main mechanisms to explain the AIE phenomenon [190].

Tetraphenylethylene (TPE) is an iconic AIE molecule. Its luminescence properties are easily affected by its own intermolecular and intramolecular movements. It is widely used to construct fluorescent probes or PSs with AIE properties. In 2015, Liu's research group built a mitochondria-targeted phototheranostic agents based on the TPE analog parent by introducing 0 (TPECM-2Br), 1 (TPECM-1TPP) or 2 (TPECM-2TPP) triphenylphosphine structures (Fig. 27a). Among these structures, TPECM-2TPP demonstrated the best mitochondrial targeting and phototherapeutic effects [191]. Next year, to enhance the targeting of phototheranostic agents to tumor cells and monitor the $^1O_2$ produced during PDT, this group used the tetrastyrene derivative TPETP as the AIE parent, $^1O_2$-cleavable aminoacrylate (AA) serves as a linker to combine a green-fluorescent rhodol dye and a functionalized CRGD moiety as tumor targeting part to make a new structure named TPETP-AA-Rho-cRGD. TPETP-AA-Rho-cRGD can realize real-time monitoring of tumor cells and the $^1O_2$ generation during PDT, and eliminating the cancer cells [192].

Generally, an increase in the energy of the HOMO or a decrease in the energy of the LUMO of the PS molecule, that is, a decrease in the HOMO-LUMO energy gap (ΔE), will lead to the red shift emission of the fluorescent molecule. It can also reduce the energy level difference (ΔE_{ST}) between S1 and T1 of the molecule, promote the ISC process, and thereby improve the PDT effect [193]. The construction of the donor-π-acceptor (D-π-A) system can reduce ΔE [194].

Li et al. constructed an AIE molecule with a D-π-A structure, TPE-TThPy, in which TPE is the electron donor, tetrahydropyridine (ThPy) is the acceptor, and thiophene (T) is the π bridge. TPE-TThPy, after being

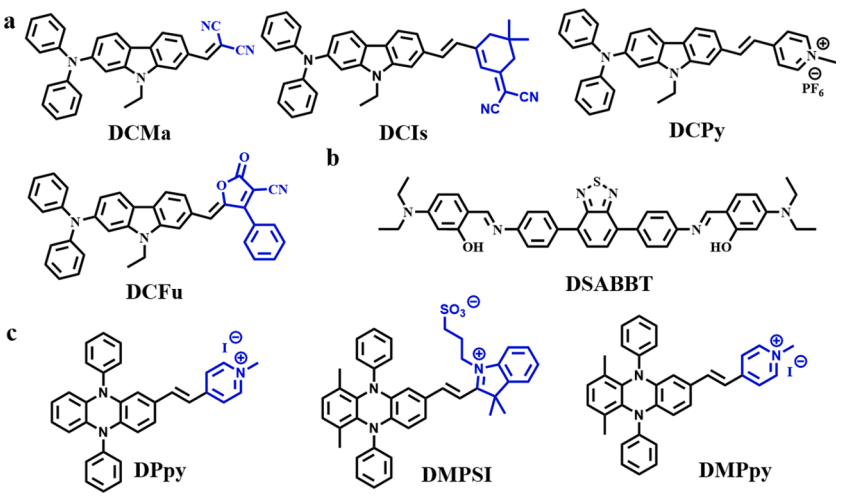

Fig. 30. Chemical structure of (a) DCMa, DCls, DCPy and DCFu; (b) DSABBT; (c) DPpy, DMPpy and DMPSI.

specifically recognized and activated by monoamine oxidase A (MAO-A), generates TPE-TPys for fluorescence imaging-guided PDT (Fig. 27b) [195]. Zhao et al., based on the above principles, introduced heavy atoms Br at the end of the alkyl chain to construct a TPTB structure, which not only achieved cell membrane localization, but also achieved synergistic treatment of type I and type II PDT (Fig. 27c) [196]. To further improve the photostability and biocompatibility of the AIE structure, Tang et al. constructed AIE NPs by wrapping two-photon AIE molecules TPE-PTB with lipids to achieve deep penetration imaging of tumor tissues (505 μm). AIE NPs can simultaneously generate $^1O_2$ and hydroxyl radicals under 800 nm illumination, achieving efficient tumor ablation (Fig. 27d) [197].

Type I PDT is of great significance in overcoming the limitations of tumor hypoxia. NIR-II fluorophores usually have deeper tissue penetration depth, negligible background fluorescence, and minimal scattering interference, which is conducive to fluorescence imaging. Not only that, NIR II photosensitizer molecules have an efficient ISC and low T_1 energy levels, promoting type I photochemical processes [198–201]. Zhao et al. used a TPE skeleton to construct TPEQM-DMA with low T_1 energy level structure through extended π conjugation and enhanced push–pull effect (Fig. 28a). TPEQM-DMA not only emit NIR-II fluorescence (>1000 nm) but also generate type I ROS (Fig. 28b and 28c). Live and dead cell staining experiments also further verified that TPEQM-DMA can exhibit highly effective anti-tumor effects under both normoxic and hypoxic conditions (Fig. 28d). The results of mouse whole-body imaging experiments show that TPEQM-DMA has excellent tumor-targeted NIR II imaging ability (Fig. 28e). As shown in Fig. 28f, the tumor growth was inhibited in TPEQM-DMA with light group [202].

6.2. *Triphenylamine-based phototheranostic agents for PDT*

Subcellular organelles are the building blocks of cells. Damage to subcellular organelle structures and functional disorders seriously affect the normal physiological processes of cells. Based on triphenylamine (TPA) derivatives, a series of subcellular organelle-targeted phototheranostic agents with AIE properties were constructed. Liu and co-workers modified the positive charged quaternary ammonium and the pyridinium structure based on the TPA parent to construct TPATrzPy-3 + with three positive charges to enhance mitochondrial targeting (Fig. 29a) [203]. Wang et al. synthesized a new compound DCMT, introduced a triphenylphosphine structure into the TPA structure to achieve mitochondrial targeting, and achieved photodiagnosis and therapy by distorting intramolecular charge transfer (Fig. 29b) [204]. Feng's team constructed a D–π–A structure TBTCP based on the TPA skeleton (Fig. 29c). This D–π–A structure is conducive to promoting ICT and ISC to increase the generation of ROS, and the positively charged pyridine structure in TBTCP is conducive to its targeting to mitochondria [205]. Quan's group also constructed a D–π–A structure TSBPy-OH based on TPA, and also introduced a pyridine structure to achieve mitochondria-targeted type I and type II synergistic PDT treatment (Fig. 29d) [206]. In the same way, Huang et al. introduced a pyridine structure into the TPA skeleton and also added a tumor cell-targeting biotin structure to construct TSPy-B to achieve dual targeting of tumor cells and mitochondria (Fig. 29e). TSPy-B with a D–π–A structure exhibits excellent type I and type II synergistic therapeutic effects [207].

Type I PDT has a significant effect on enhancing the therapeutic effect of hypoxic tumors. Qi and co-workers constructed a D–π–A structure CTQ-S with type I PDT effect. TPA serves as the electron donor, and quinolinium salt serves as the electron acceptor (Fig. 29f). It has found that the longer the π conjugation length, the more conducive to ISC. The introduction of quinoline salt is conducive to creating an electron-rich environment, which is conducive to the T_1 state to achieve free radicals' production through type I electron transfer. CTQ-S targets migration from the cell membrane to mitochondria over time [208]. Feng et al. also constructed type I D-D-A structure MTOTPy, using TPA as the electron donor, electron-withdrawing pyridinium as the electron acceptor, and 3,4 ethylenedioxy-thiophene as the electron donor and π bridge (Fig. 29g). This structure promotes the separation of HOMO-LUMO distribution, resulting in more ICT to reduce ΔE_{ST} to generate more ROS. 3,4 ethylenedioxythiophene is a strong electron donor that promotes MTOTPy to produce free radicals from type I PDT process [209].

Based on the above reports, Liu and co-workers designed an AIE structure, ADB, for dual targeting of lysosomes and mitochondria (Fig. 29h). ADB is a D-A-π-A structure with TPA as the electron donor, 2,1,3-benzothiadiazole and 2,3-dimethylbenzo[d]thiazole-3-onium iodide groups as a combined electron acceptor. ADB nanoparticles can target lysosomes and mitochondria [210]. To construct a cell membrane-targeted AIE phototheranostic agent, Tang et al. designed a D-A compound TTVP, which contains triphenylamine fragments and thiophene fragments as electron donors, carbon–carbon double bonds as π bridges, and pyridinium as electron acceptors (Fig. 29i). TTVP is water-soluble and can be used for ultrafast membrane-targeted imaging [211].

Lipid droplets (LDs) are lipid-rich organelles that regulate the storage and hydrolysis of neutral lipids. They also serve as a reservoir of cholesterol and glycerides for membrane formation and maintenance [212]. Qi et al. constructed a MeTTSN molecule with a D-π-A structure using TPA as the electron donor, benzothiazole 2-acetonitrile as the electron accepting group, and thiophene as the π bridge (Fig. 29j).

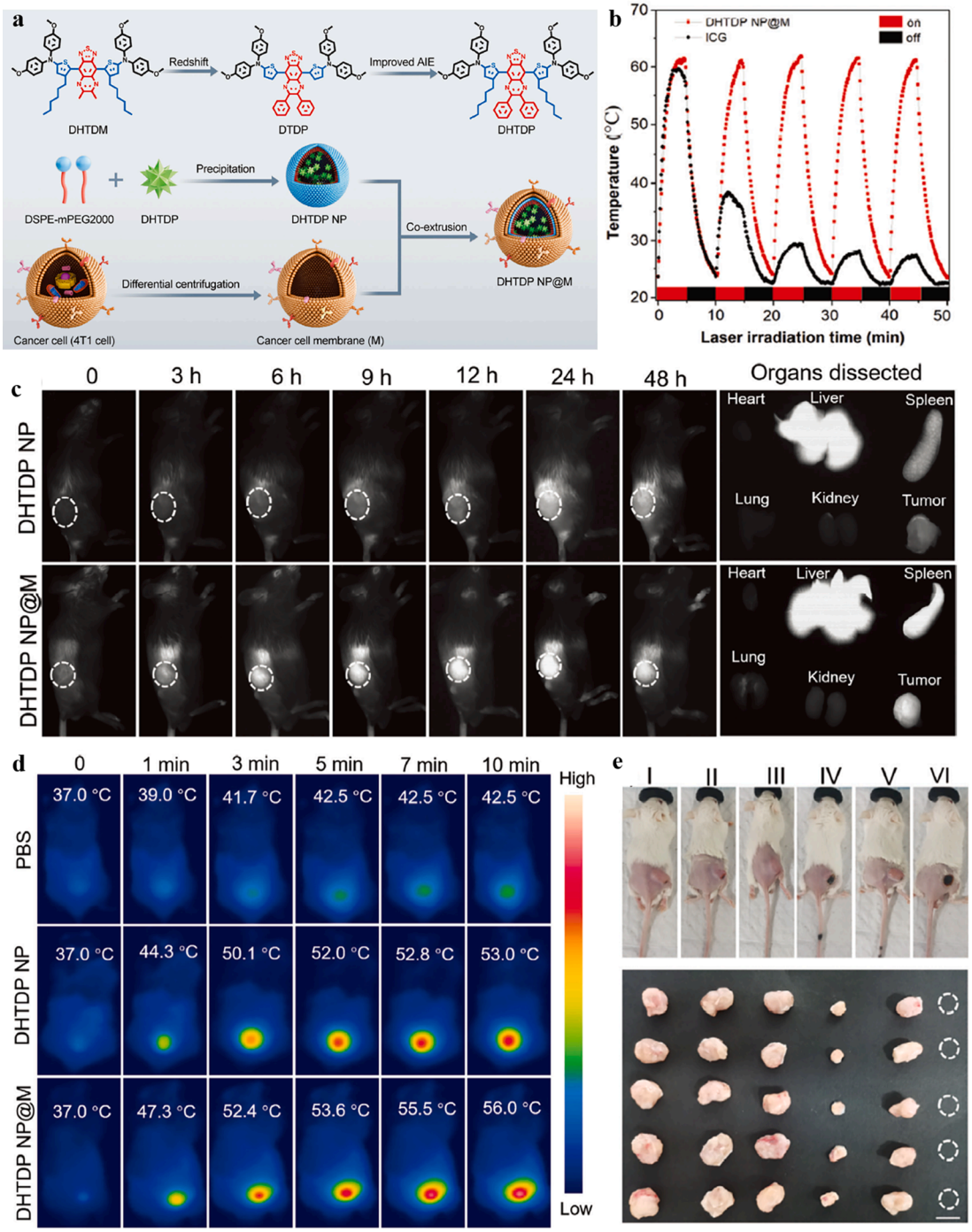

Fig. 31. (a) Chemical structure of NHTDP and nanostructure of NHTDP@M. (b) Photothermal effect and photostability of DHTDP NP@M (c) In vivo NIR-II fluorescence imaging of tumor-bearing mice after injection of DHTDP NP and DHTDP NP@M. (d) Time-depended photothermal imaging *in vivo*. (e) Tumor growth of mice after various treatments. Reprinted with permission from Ref. [222], copyright © 2023 Wiley-VCH GmbH.

MeTTSN can detect lipid droplets and eliminate tumor cells [213]. Different from "always on" phototherapy agents, Hua's group constructed an activatable AIE molecule, DPP-BPYS, for H_2O_2-activated lipid droplet-targeted phototherapy (Fig. 29k). DPP-BPYS uses methoxy-substituted TPA as a strong electron donor, pyridyl-modified diketopyrrolopyrrole as an electron acceptor, and adds a freely rotating benzene ring to further inhibit π-π stacking, the p-pinacolborylbenzyl moiety is connected to the pyridine group of DPP-BPY, thus forming an activatable AIE phototheranostic agent with selective response to H_2O_2 [214].

6.3. Other AIEgens for PDT

Electron-donating diphenylamine groups connected to electron-rich carbazolyl ring derivatives are also widely used as AIE precursors [215–217]. Tang's group synthesized a series of molecules with AIE function. The electron-donating diphenylamine group is connected to four different electron-withdrawing groups (malononitrile, isophorone, picolinium salt, and 3-cyano-4-phenyl-2(5H)-furanone) to construct DCMa, DCIs, DCPy and DCFu respectively (Fig. 30a). The cationic DCPy can achieve mitochondrial targeting, and the other three molecules can achieve lipid droplet targeting. The NIR and far-infrared emission of AIE

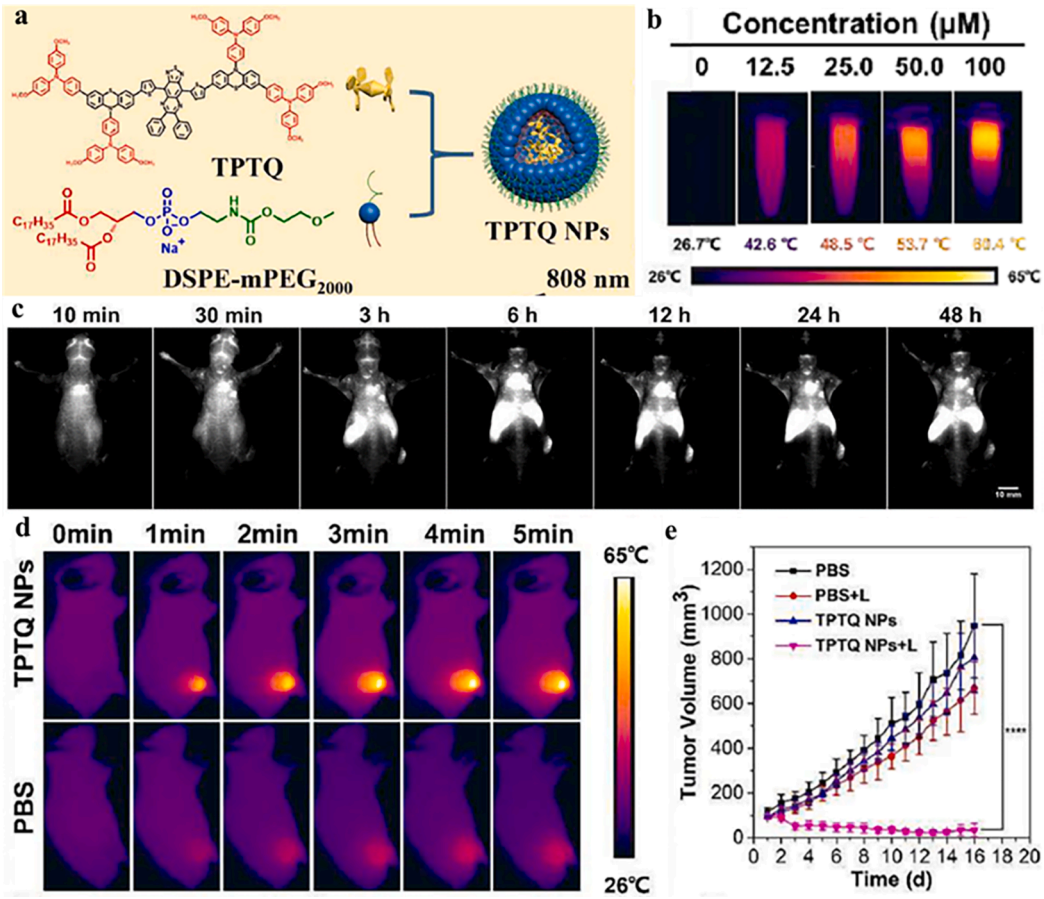

Fig. 32. (a) Chemical structure of TPTQ and nanostructure of TPTQ NPs. (b) Photothermal effect TPTQ NPs (c) In vivo NIR-II fluorescence imaging of tumor-bearing mice after injection of TPTQ NPs. (d) Time-depended photothermal imaging *in vivo*. (e) Tumor growth of mice after various treatments. Reprinted with permission from Ref. [223], copyright © 2023 Elsevier B.V. All rights reserved.

molecules is controlled by introducing different strong electron acceptors [217]. Wei et al. synthesized DSABBT with AIE properties by using 4-(diethylamino)-salicylaldehyde and 4,7-bis(4-aminophenyl)-2,1,3-benzothiadiazole through a one-step reaction (Fig. 30b). DSABBT was further assembled with the tumor-targeting polymer DSPE-PEG2000-cRGD to construct nanoparticles that can be used for two-photon fluorescence imaging-guided PDT [218]. Based on N,N'-diphenyldihydrophenazine and its *ortho*-dimethyl-substituted derivative DMP, Hua et al. designed and synthesized three D-A structure cyanine dyes DPpy, DMPpy and DMPSI (Fig. 30c). Strong electron donor and acceptor to enhance ICT, which is beneficial to promote type I PDT process. Among these three dyes, DMPpy based on DMP linked to styrylpyridinium iodide exhibits AIE properties, excellent type I PDT efficiency, bright NIR emission (approximately 700 nm) and mitochondrial targeting ability [219].

6.4. AIEgens for PTT

How to balance the competition between radiation-mediated fluorescence imaging and non-radiation PTT is an important challenge in constructing fluorescence-imaging guided PTT [220,221]. The balance between radiative and non-radiative energy dissipation of phototheranostic agents can be adjusted by regulating intramolecular interactions and distortion of molecular structures. Based on this, Tang's group prepared 5,5′-(6,7-diphenyl-[1,2,5]thiadiazolo[3,4–g]quinoxaline-4,9-diyl)bis(4-hexyl-N,N-bis(4-methoxyphenyl)thiophen-2-amine) (DHTDP), realizes NIR absorption and NIR II fluorescence emission, increases fluorescence penetration depth and control of PCE. To further improve tumor targeting, NHTDP nanomaterials were assembled using 4 T1 cell membranes to construct tumor cell membrane biomimetic nanomaterials NHTDP@M (Fig. 31a). As shown in Fig. 31b, NHTDP@M exhibits excellent photothermal properties and photostability. Whole-body NIR II fluorescence imaging in tumor-bearing mice suggested that the tumor targeting ability was improved after assembly with tumor cell membranes (Fig. 31c). In vivo photothermal imaging results in mice showed that after 10 min of 808 nm laser irradiation, the temperature of the NHTDP@M group increased to 56 °C, which could effectively ablate tumors (Fig. 31d and 31e).[222].

Huang et al. proposed a new design strategy to improve PTT: planarized acceptors, π bridges and rotating donors. The planarization of π bridges and acceptor units helps to enhance the ICT effect and introduce more electron-donating groups, resulting in red-shifted absorption and fluorescence emission. Introducing a rotating donor prevents aggregation-induced fluorescence quenching, and facilitates the continued rotation of the internal rotor to expand nonradiative transitions. Based on the above strategy, TPTQ was successfully constructed, with the strong electron-withdrawing 6, 7-diphenyl-[1,2,5]thiadiazolo [3,4g]quinoxaline as the acceptor, thiophene as the π bridge, phenothiazine serves as the acceptor, and a triphenylamine rotor donor is added to the phenothiazine (Fig. 32a). TPTQ shows excellent photothermal conversion capabilities, and the calculated PCE can reach 73.32 % (Fig. 32b). The whole-body NIR II fluorescence imaging experiment of TPTQ in tumor-bearing mice showed that TPTQ can visually image the tumor site (Fig. 32c). After being exposed to 808 nm laser, the temperature of the tumor site is as high as 60 °C, which is conducive to the thermal ablation of tumors (Fig. 32d and 32e) [223].

7. Conclusions and perspectives

In this review, we summarized the organic molecules inculding cyanines, porphyrins, phthalocyanines, BODIPY, and AIEgens or nanoaggregates and nanocomposite based on these organic molecules for fluorescence imaging-guided phototherapy. Special attention is paid to the strategy of visual elimination of tumors through molecular structure modification, controlled aggregation, and assembly of functionalized nanomaterials. Obviously, this integrated approach to diagnosis and treatment demonstrates the huge potential for clinical transformation of precision tumor treatment. However, fluorescence imaging-guided phototherapy for tumor elimination still faces great challenges: (1) There is currently no fully mature method that can accurately control the fluorescence, photodynamic or photothermal intensity of all kinds of PSs. The strategies used by different PSs molecules are not completely consistent, and the design methods need to be adjusted according to the structure. (2) Maintaining photostability of fluorescence after continuous high-intensity output is a huge challenge. Meanwhile, fluorescence imaging will also face interference from background. To solve the above problems, some afterglow luminescent structures have been studied. Such structures store the energy of the illuminated light and then slowly emit photons. Song et al. have achieved tumor glycolysis and chemotherapy resistance by constructing afterglow structure; [224] in addition, this kind of materials can also quantify and image targets such as pH, superoxide anion, and aminopeptidase [225]. (3) Quantitatively evaluating the accuracy of detecting early tumor lesions through fluorescence intensity and the effectiveness of phototherapy is still limited. (4) The problem of penetration depth. There is an urgent need to further expand the fluorescence emission wavelength so that it can be used for the visual treatment of deep-seated solid tumors. Currently, photoacoustic imaging is favored due to its deeper penetration depth [226]. In addition to tumors, diseases such as atherosclerosis can also be diagnosed early through photoacoustic imaging [227,228]. (5) Phototherapy has the disadvantage of locality, and metastatic tumors are difficult to detect or treat through this method. In this case, phototherapy needs to be used in conjunction with systemic treatments such as chemotherapy and immunotherapy to enhance the therapeutic effect of metastatic tumors.

Collectively, the use of fluorescence-imaging guided phototherapy for anti-tumor is a promising strategy. This review summarizes the progress made in this field in recent years as well as the opportunities and challenges faced. We believe that with the continuous efforts of scientific researchers and clinicians, fluorescence imaging-guided phototherapy will become a prominent feature in the field of precision tumor treatment in the future.

Declaration of competing interest

The authors declare that they have no known competing financial interests or personal relationships that could have appeared to influence the work reported in this paper.

Data availability

No data was used for the research described in the article.

Acknowledgements

This work was supported by the Hainan Provincial Natural Science Foundation of China (823MS050, 824QN270), Education Department of Hainan Province (Hnky2023ZD-11, Hnky2023ZD-12), National Natural Science Foundation of China (22264013, 82360417) and Hainan Province Science and Technology Special Fund (Grant ZDYF2020133, ZDYF2024SHFZ131).

References

[1] R.L. Siegel, K.D. Miller, N.S. Wagle, A. Jemal, Ca Cancer J. Clin. 73 (2023) 17–48.
[2] D. Xu, J. Ge, Y. An, S. Bai, Z. Wang, S. Wu, Q. Dai, Z. Lu, G. Liu, Small 19 (2023) e2300859.
[3] C.A. Klein, Nat. Rev. Cancer 20 (2020) 681–694.
[4] X. Li, J.F. Lovell, J. Yoon, X. Chen, Nat. Rev. Clin. Oncol. 17 (2020) 657–674.
[5] W. Fan, B. Yung, P. Huang, X. Chen, Chem. Rev. 117 (2017) 13566–13638.
[6] K. Ni, G. Lan, S.S. Veroneau, X. Duan, Y. Song, W. Lin, Nat. Commun. 9 (2018) 4321.
[7] H. Chen, W. Zhang, G. Zhu, J. Xie, X. Chen, Nat. Rev. Mater. 2 (2017) 1–18.
[8] H. Xie, Z. Bi, J. Yin, Z. Li, L. Hu, C. Zhang, J. Zhang, J.W.Y. Lam, P. Zhang, R.T. K. Kwok, K. Li, B.Z. Tang, ACS Nano 17 (2023) 4591–4600.
[9] L. Shi, Y. Wang, C. Zhang, Y. Zhao, C. Lu, B. Yin, Y. Yang, X. Gong, L. Teng, Y. Liu, Angew. Chem. Int. Ed. 133 (2021) 9648–9658.
[10] C. Lu, C. Zhang, P. Wang, Y. Zhao, Y. Yang, Y. Wang, H. Yuan, S. Qu, X. Zhang, G. Song, Chem 6 (2020) 2314–2334.
[11] H. Kim, M. Yang, N. Kwon, M. Cho, J. Han, R. Wang, S. Qi, H. Li, V.N. Nguyen, X. Li, Bull. Korean Chem. Soc. 44 (2023) 236–255.
[12] Z. Li, Z. Zhou, Y. Wang, J. Wang, L. Zhou, H.-B. Cheng, J. Yoon, Coord. Chem. Rev. 493 (2023) 215324.
[13] A.F. dos Santos, D.Q. de Almeida, L.F. Terra, M.S. Baptista, L. Labriola, J. Cancer Metastasis Treat. 5 (2019) 10.20517.
[14] H. Kim, Y.R. Lee, H. Jeong, J. Lee, X. Wu, H. Li, J. Yoon, Smart Molecules (2023) e20220010.
[15] V.-N. Nguyen, Z. Zhao, B.Z. Tang, J. Yoon, Chem. Soc. Rev. 51 (2022) 3324–3340.
[16] R. Wang, D. Kim, M. Yang, X. Li, J. Yoon, ACS Appl. Mater. Inter. 14 (2022) 7609–7616.
[17] Z. Zhou, J. Song, L. Nie, X. Chen, Chem. Soc. Rev. 45 (2016) 6597–6626.
[18] P. Mroz, A. Yaroslavsky, G.B. Kharkwal, M.R. Hamblin, Cancers 3 (2011) 2516–2539.
[19] P. Agostinis, K. Berg, K.A. Cengel, T.H. Foster, A.W. Girotti, S.O. Gollnick, S. M. Hahn, M.R. Hamblin, A. Juzeniene, D. Kessel, Ca,, Cancer J. for Clin. 61 (2011) 250–281.
[20] G. Feng, G.-Q. Zhang, D. Ding, Chem. Soc. Rev. 49 (2020) 8179–8234.
[21] Y. Yao, P. Ding, C. Yan, Y. Tao, B. Peng, W. Liu, J. Wang, M.A. Cohen Stuart, Z. Guo, Angew. Chem. Int. Ed. 62 (2023) e202218983.
[22] H. Shen, B. Wu, Q. Zhang, J. Ni, M. Liang, Y. Liu, X.-F. Zang, S. Wang, Y.-Y. Quan, X. Ye, Z.-S. Huang, Chem. Eng. J. 468 (2023) 143726.
[23] L. Cheng, C. Wang, L. Feng, K. Yang, Z. Liu, Chem. Rev. 114 (2014) 10869–10939.
[24] W. Zhu, M. Kang, Q. Wu, Z. Zhang, Y. Wu, C. Li, K. Li, L. Wang, D. Wang, B. Z. Tang, Adv. Funct. Mater. 31 (2021) 2007026.
[25] X. Wu, R. Wang, N. Kwon, H. Ma, J. Yoon, Chem. Soc. Rev. 51 (2022) 450–463.
[26] R. Wang, X. Han, J. You, F. Yu, L. Chen, Anal. Chem. 90 (2018) 4054–4061.
[27] M. Gao, F. Yu, C. Lv, J. Choo, L. Chen, Chem. Soc. Rev. 46 (2017) 2237–2271.
[28] D. Wu, Z. Zhao, N. Wang, X. Zhang, H. Yan, X. Chen, Y. Fan, W. Liu, X. Liu, Biomaterials Science 8 (2020) 3443–3453.
[29] H. Li, D. Kim, Q. Yao, H. Ge, J. Chung, J. Fan, J. Wang, X. Peng, J. Yoon, Angew. Chem. Int. Ed. 133 (2021) 17408–17429.
[30] C. Yan, Y. Zhang, Z. Guo, Coord. Chem. Rev. 427 (2021) 213556.
[31] R.R. Zhang, A.B. Schroeder, J.J. Grudzinski, E.L. Rosenthal, J.M. Warram, A. N. Pinchuk, K.W. Eliceiri, J.S. Kuo, J.P. Weichert, Nat. Rev. Clin. Oncol. 14 (2017) 347–364.
[32] C. Wang, Z. Wang, T. Zhao, Y. Li, G. Huang, B.D. Sumer, J. Gao, Biomaterials 157 (2018) 62–75.
[33] X. Li, B.-D. Zheng, X.-H. Peng, S.-Z. Li, J.-W. Ying, Y. Zhao, J.-D. Huang, J. Yoon, Coord. Chem. Rev. 379 (2019) 147–160.
[34] A. Kamkaew, S.H. Lim, H.B. Lee, L.V. Kiew, L.Y. Chung, K. Burgess, Chem. Soc. Rev. 42 (2013) 77–88.
[35] X. Li, J. Kim, J. Yoon, X. Chen, Adv. Mater. 29 (2017) 1606857.
[36] S.S. Lucky, K.C. Soo, Y. Zhang, Chem. Rev. 115 (2015) 1990–2042.
[37] W. Fan, P. Huang, X. Chen, Chem. Soc. Rev. 45 (2016) 6488–6519.
[38] J. Zhou, L. Rao, G. Yu, T.R. Cook, X. Chen, F. Huang, Chem. Soc. Rev. 50 (2021) 2839–2891.
[39] C. Chen, H. Ou, R. Liu, D. Ding, Adv. Mater. 32 (2020) 1806331.
[40] G. Gao, X. Sun, G. Liang, Adv. Funct. Mater. 31 (2021) 2100738.
[41] J.A. Carr, D. Franke, J.R. Caram, C.F. Perkinson, M. Saif, V. Askoxylakis, M. Datta, D. Fukumura, R.K. Jain, M.G. Bawendi, Proc. Natl. Acad. Sci. U.S.A. 115 (2018) 4465–4470.
[42] W. Sun, S. Guo, C. Hu, J. Fan, X. Peng, Chem. Rev. 116 (2016) 7768–7817.
[43] X. Zhao, H. Zhao, S. Wang, Z. Fan, Y. Ma, Y. Yin, W. Wang, R. Xi, M. Meng, J. Am. Chem. Soc. 143 (2021) 20828–20836.
[44] J. He, Y. Wang, M.A. Missinato, E. Onuoha, L.A. Perkins, S.C. Watkins, C.M. St Croix, M. Tsang, M.P. Bruchez, Nat. Methods 13 (2016) 263–268.
[45] C. Pontremoli, G. Chinigò, S. Galliano, M.M. Plata, D. Dereje, E. Sansone, A. Gilardino, C. Barolo, A.F. Pla, S. Visentin, Dyes Pigm. 210 (2023) 111047.
[46] J. Atchison, S. Kamila, H. Nesbitt, K.A. Logan, D.M. Nicholas, C. Fowley, J. Davis, B. Callan, A.P. McHale, J.F. Callan, Chem. Comm. 53 (2017) 2009–2012.
[47] D. Kobzev, O. Semenova, A. Tatarets, A. Bazylevich, G. Gellerman, L. Patsenker, Dyes Pigm. 212 (2023) 111101.
[48] T. Hompland, C.S. Fjeldbo, H. Lyng, Cancers 13 (2021) 499.
[49] M. Li, T. Xiong, J. Du, R. Tian, M. Xiao, L. Guo, S. Long, J. Fan, W. Sun, K. Shao, J. Am. Chem. Soc. 141 (2019) 2695–2702.

[50] T.J. Dougherty, C.J. Gomer, B.W. Henderson, G. Jori, D. Kessel, M. Korbelik, J. Moan, Q. Peng, J. Natl. Cancer Inst. 90 (1998) 889–905.
[51] Y.C. Liu, G.J. Liu, W. Zhou, G.L. Feng, Q.Y. Ma, Y. Zhang, G.W. Xing, Angew. Chem. Int. Ed. 135 (2023) e202309786.
[52] Y. Zhang, M. Zhao, J. Miao, W. Gu, J. Zhu, B. Cheng, Q. Li, Q. Miao, A.C.S. Mater, Lett. 5 (2023) 3058–3067.
[53] S.H. Lim, C. Thivierge, P. Nowak-Sliwinska, J. Han, H. van den Bergh, G. Wagnieres, K. Burgess, H.B. Lee, J. Med. Chem. 53 (2010) 2865–2874.
[54] T.C. Pham, V.-N. Nguyen, Y. Choi, S. Lee, J. Yoon, Chem. Rev. 121 (2021) 13454–13619.
[55] L. Jiao, F. Song, J. Cui, X. Peng, Chem. Comm. 54 (2018) 9198–9201.
[56] H. Ma, S. Long, J. Cao, F. Xu, P. Zhou, G. Zeng, X. Zhou, C. Shi, W. Sun, J. Du, Chem. Sci. 12 (2021) 13809–13816.
[57] K. Hanaoka, S. Iwaki, K. Yagi, T. Myochin, T. Ikeno, H. Ohno, E. Sasaki, T. Komatsu, T. Ueno, M. Uchigashima, J. Am. Chem. Soc. 144 (2022) 19778–19790.
[58] J. Miao, Y. Huo, G. Yao, Y. Feng, J. Weng, W. Zhao, W. Guo, Angew. Chem. Int. Ed. 61 (2022) e202201815.
[59] S. Chen, L. Xiao, Y. Li, M. Qiu, Y. Yuan, R. Zhou, C. Li, L. Zhang, Z.X. Jiang, M. Liu, Angew. Chem. Int. Ed. 134 (2022) e202213495.
[60] F. Han, S.A. Abbas Abedi, S. He, H. Zhang, S. Long, X. Zhou, S. Chanmungkalakul, H. Ma, W. Sun, X. Liu, J. Du, J. Fan, X. Peng, Adv. Sci. (2023) 2305761.
[61] C. Lu, Z. Li, N. Wu, D. Lu, X.-B. Zhang, G. Song, Chem 9 (2023) 3185–3211.
[62] X. Meng, Y. Yang, L. Zhou, Y. Lv, S. Li, Y. Wu, M. Zheng, W. Li, G. Gao, G. Deng, Theranostics 7 (2017) 1781–1794.
[63] R. Wang, X. Li, J. Yoon, ACS Appl. Mater. Inter. 13 (2021) 19543–19571.
[64] Z. Cai, J. Yu, J. Hu, K. Sun, M. Liu, D. Gu, J. Chen, Y. Xu, X. He, W. Wei, Spectrochimica Acta Part a: Mol. Biomol. Spectrosc. 286 (2023) 122027.
[65] W. Zhou, S. Chen, Y. Ouyang, B. Huang, H. Zhang, W. Zhang, J. Tian, Chem. Sci. 14 (2023) 11481–11489.
[66] H. Zhang, C. Shi, F. Han, L. Cai, H. Ma, S. Long, W. Sun, J. Du, J. Fan, X. Chen, Biomaterials 302 (2023) 122365.
[67] K. Wei, Y. Wu, X. Zheng, G. Ma, C. Ji, M. Yin, Adv. Funct. Mater. 33 (2023) 2305187.
[68] Y. Cai, Z. Wei, C. Song, C. Tang, W. Han, X. Dong, Chem. Soc. Rev. 48 (2019) 22–37.
[69] C. Zhu, L. Liu, Q. Yang, F. Lv, S. Wang, Chem. Rev. 112 (2012) 4687–4735.
[70] Y. Tian, Z. Chen, S. Liu, F. Wu, W. Cao, D.W. Pang, H. Xiong, Angew Chem. Int. Ed. 62 (2023) e202309768.
[71] J.M. Brown, W.R. Wilson, Nat. Rev. Cancer 4 (2004) 437–447.
[72] K. Okuda, Y. Okabe, T. Kadonosono, T. Ueno, B.G. Youssif, S. Kizaka-Kondoh, H. Nagasawa, Bioconjug. Chem. 23 (2012) 324–329.
[73] X. Meng, J. Zhang, Z. Sun, L. Zhou, G. Deng, S. Li, W. Li, P. Gong, L. Cai, Theranostics 8 (2018) 6025–6034.
[74] J. Zhang, Z. Liu, P. Lian, J. Qian, X. Li, L. Wang, W. Fu, L. Chen, X. Wei, C. Li, Chem. Sci. 7 (2016) 5995–6005.
[75] N.V. Belko, G.A. Gusakov, S.K. Poznyak, S.A. Tikhomirov, A.P. Lugovski, M. P. Samtsov, J. Phys. Chem. C 126 (2022) 7922–7932.
[76] W. Chen, C.-A. Cheng, E.D. Cosco, S. Ramakrishnan, J.G. Lingg, O.T. Bruns, J. I. Zink, E.M. Sletten, J. Am. Chem. Soc. 141 (2019) 12475–12480.
[77] X. Ma, Y. Huang, W. Chen, J. Liu, S.H. Liu, J. Yin, G.F. Yang, Angew. Chem. Int. Ed. 62 (2023) e202216109.
[78] N.J. Hestand, F.C. Spano, Chem. Rev. 118 (2018) 7069–7163.
[79] K. Wei, Y. Wu, P. Li, X. Zheng, C. Ji, M. Yin, Nano Res. 16 (2023) 970–979.
[80] F. Wu, Y. Lu, X. Mu, Z. Chen, S. Liu, X. Zhou, S. Liu, Z. Li, ACS Appl. Mater. Inter. 12 (2020) 32388–32396.
[81] K. Tang, S. Jia, Y. Zou, J. Dong, F. Liu, K. Cui, X. Shi, L. Zhang, Gene Protein Dis. 1 (2022) 87.
[82] H. Qian, Q. Cheng, Y. Tian, H. Dang, C. Teng, L. Yan, J. Mater. Chem. B 9 (2021) 2688–2696.
[83] J. Fang, H. Nakamura, H. Maeda, Adv. Drug Deliv. Rev. 63 (2011) 136–151.
[84] V.C. Jordan, Breast Cancer Management 3 (2014) 321–326.
[85] V.C. Jordan, Nat. Rev. Drug Discov. 2 (2003) 205–213.
[86] Y. Zou, M. Li, T. Xiong, X. Zhao, J. Du, J. Fan, X. Peng, Small 16 (2020) 1907677.
[87] Y. Wu, W. Zhang, D. Xu, L. Ding, R. Ma, J.-Z. Wu, J.-H. Tang, Lasers Med. Sci. 33 (2018) 1601–1608.
[88] X. Meng, W. Li, Z. Sun, J. Zhang, L. Zhou, G. Deng, P. Gong, L. Cai, J. Mater, Chem. B 5 (2017) 9405–9411.
[89] G.-Y. Pan, H.-R. Jia, Y.-X. Zhu, R.-H. Wang, F.-G. Wu, Z. Chen, ACS Biomater. Sci. Eng. 3 (2017) 3596–3606.
[90] A. St, E.R. Lorenz, O. Buabeng, O. Taratula, M.H. Taratula, J. Med. Chem. 64 (2021) 8798–8805.
[91] G. Jo, E.J. Kim, H. Hyun, Int. J. Mol. Sci 24 (2023) 862.
[92] J. Zhu, G. He, P.-H. Chen, Y. Zhang, Y. Zhang, S. Lei, Y. Zhang, M. Li, P. Huang, J. Lin, Research 6 (2023) 0061.
[93] S. Lei, F. Zhao, J. Zhang, N.T. Blum, T. He, J. Qu, P. Huang, J. Lin, Anal. Chem. 94 (2022) 8399–8408.
[94] Z. Zhang, R. Wang, X. Huang, R. Luo, J. Xue, J. Gao, W. Liu, F. Liu, F. Feng, W. Qu, ACS Appl. Mater. Inter. 12 (2020) 5680–5694.
[95] R. Zhao, X. Han, Y. Li, H. Wang, T. Ji, Y. Zhao, G. Nie, ACS Nano 11 (2017) 8103–8113.
[96] T. Desmettre, J. Devoisselle, S. Mordon, Surv. Ophthalmol. 45 (2000) 15–27.
[97] C. Shirata, J. Kaneko, Y. Inagaki, T. Kokudo, M. Sato, S. Kiritani, N. Akamatsu, J. Arita, Y. Sakamoto, K. Hasegawa, Sci. Rep. 7 (2017) 13958.
[98] J. Cao, J. Chi, J. Xia, Y. Zhang, S. Han, Y. Sun, ACS Appl. Mater. Inter. 11 (2019) 25720–25729.
[99] J. Chen, X. Tan, S. Luo, L. Long, L. Liu, Z. Liu, Y. Wang, C. Shi, J. Innov. Opt. Health Sci. 11 (2018) 1850016.
[100] M. Gao, X. Huang, Z. Wu, L. Wang, S. Yuan, Z. Du, S. Luo, R. Li, W. Wang, Materials Today Bio 15 (2022) 100316.
[101] S. Luo, X. Tan, S. Fang, Y. Wang, T. Liu, X. Wang, Y. Yuan, H. Sun, Q. Qi, C. Shi, Adv. Funct. Mater 26 (2016) 2826–2835.
[102] Q.-S. Gu, T. Li, W.-X. Wang, Z.-Q. Wang, Q.-R. Liu, G.-J. Mao, Y. Li, C.-Y. Li, Sens. Actuators B Chem. 393 (2023) 134287.
[103] Y. Xu, J. Yu, J. Hu, K. Sun, W. Lu, F. Zeng, J. Chen, M. Liu, Z. Cai, X. He, Adv. Healthc. Mater. (2023) 2203080.
[104] Y. Li, Y. Sun, J. Li, Q. Su, W. Yuan, Y. Dai, C. Han, Q. Wang, W. Feng, F. Li, J. Am. Chem. Soc. 137 (2015) 6407–6416.
[105] X. Zhao, S. Long, M. Li, J. Cao, Y. Li, L. Guo, W. Sun, J. Du, J. Fan, X. Peng, J. Am. Chem. Soc. 142 (2019) 1510–1517.
[106] Y. Dong, L. Zhou, Z. Shen, Q. Ma, Y. Zhao, Y. Sun, J. Cao, Drug Deliv. 29 (2022) 238–253.
[107] J. Chi, Q. Ma, Z. Shen, C. Ma, W. Zhu, S. Han, Y. Liang, J. Cao, Y. Sun, Nanoscale 12 (2020) 11008–11025.
[108] W.-N. Zeng, Q.-P. Yu, D. Wang, J.-L. Liu, Q.-J. Yang, Z.-K. Zhou, Y.-P. Zeng, J. Nanobiotechnology 19 (2021) 1–19.
[109] C. Huang, Z. Zhang, Q. Guo, L. Zhang, F. Fan, Y. Qin, H. Wang, S. Zhou, W. Ou-Yang, H. Sun, Adv. Healthc. Mater. 8 (2019) 1900840.
[110] M. Liang, X. Mu, Y. Li, Y. Tan, X. Hao, Y. Tang, Z. Wang, W. Feng, Y. Lu, X. Zhou, Adv. Funct. Mater. 33 (2023) 2302112.
[111] T. Liu, Y. Chen, H. Wang, M. Cui, J. Zhang, W. Zhang, P. Wang, Adv. Healthc. Mater. 12 (2023) 2202817.
[112] X. Zhao, K.-K. Zhang, L.-J. Chen, Z.-Y. Wang, X.-P. Yan, ACS Appl. Nano Mater. 6 (2023) 10501–10510.
[113] Y. Li, J. Zhang, L. Zhu, M. Jiang, C. Ke, H. Long, R. Lin, C. Ye, X. Zhou, Z.X. Jiang, Adv. Healthc. Mater. (2023) 2300941.
[114] J.V. Gregory, P. Kadiyala, R. Doherty, M. Cadena, S. Habeel, E. Ruoslahti, P. R. Lowenstein, M.G. Castro, J. Lahann, Nat. Commun. 11 (2020) 5687.
[115] E.R. Fearon, B. Vogelstein, Cell 61 (1990) 759–767.
[116] Z. Hu, R. Li, X. Cui, Z. Chen, ACS Appl. Mater. Inter. 15 (2023) 33890–33902.
[117] J.M. Park, K.-I. Hong, H. Lee, W.-D. Jang, Acc. Chem. Res. 54 (2021) 2249–2260.
[118] H. Mori, T. Tanaka, A. Osuka, J. Mater. Chem. C 1 (2013) 2500–2519.
[119] S. Guo, D. Gu, Y. Yang, J. Tian, X. Chen, J. Nanobiotechnology 21 (2023) 348.
[120] X. Li, X.-H. Peng, B.-D. Zheng, J. Tang, Y. Zhao, B.-Y. Zheng, M.-R. Ke, J.-D. Huang, Chem. Sci. 9 (2018) 2098–2104.
[121] R. Wang, K.-H. Kim, J. Yoo, X. Li, N. Kwon, Y.-H. Jeon, S.-K. Shin, S.S. Han, D.-S. Lee, J. Yoon, ACS Nano 16 (2022) 3045–3058.
[122] H. Sun, R. Guo, Y. Guo, J. Song, Z. Li, F. Song, Mol. Pharm. 20 (2022) 606–615.
[123] X. Liang, M. Chen, P. Bhattarai, S. Hameed, Z. Dai, ACS Nano 14 (2020) 13569–13583.
[124] X. Liu, L. Chen, Z. Chen, Bioorg. Chem. 143 (2024) 106986.
[125] X. Liu, W. Zhan, G. Gao, Q. Jiang, X. Zhang, H. Zhang, X. Sun, W. Han, F.-G. Wu, G. Liang, J. Am. Chem. Soc. 145 (2023) 7918–7930.
[126] K.S. Crider, T.P. Yang, R.J. Berry, L.B. Bailey, Adv. Nutr. 3 (2012) 21–38.
[127] Y. Chen, W. Liu, Y. Shang, P. Cao, J. Cui, Z. Li, X. Yin, Y. Li, Int. J. Nanomedicine (2019) 57–74.
[128] A.J. Ablooglu, J. Kang, B.G. Petrich, M.H. Ginsberg, S.J. Shattil, Blood 113 (2009) 3585–3592.
[129] Y. Shang, H. Zhang, Y. Cheng, P. Cao, J. Cui, X. Yin, S. Fan, Y. Li, Int. J. Nanomedicine (2022) 1381–1395.
[130] B.-Y. Zheng, X.-Q. Yang, Y. Zhao, Q.-F. Zheng, M.-R. Ke, T. Lin, R.-X. Chen, K. K. Ho, N. Kumar, J.-D. Huang, Eur. J. Med. Chem. 155 (2018) 24–33.
[131] S.Y. Ha, R.C. Wong, C.T. Wong, D.K. Ng, Eur. J. Med. Chem 174 (2019) 56–65.
[132] S. Chen, X. Zhao, J. Chen, J. Chen, L. Kuznetsova, S.S. Wong, I. Ojima, Bioconjug. Chem. 21 (2010) 979–987.
[133] K. Li, L. Qiu, Q. Liu, G. Lv, X. Zhao, S. Wang, J. Lin, J. Photochem. Photobiol. b, Biol. 174 (2017) 243–250.
[134] K. Li, W. Dong, Q. Liu, G. Lv, M. Xie, X. Sun, L. Qiu, J. Lin, J. Photochem. Photobiol. b, Biol. 190 (2019) 1–7.
[135] G. Avşar, F.A. Sari, A.C. Yuzer, H.M. Soylu, O. Er, M. Ince, F.Y. Lambrecht, Int. J. Pharmaceut. 505 (2016) 369–375.
[136] Z. Zhao, P.-S. Chan, H. Li, K.-L. Wong, R.N.S. Wong, N.-K. Mak, J. Zhang, H.-L. Tam, W.-Y. Wong, D.W. Kwong, Inorg. Chem. 51 (2012) 812–821.
[137] D. Pan, P. Liang, X. Zhong, D. Wang, H. Cao, W. Wang, W. He, Z. Yang, X. Dong, ACS Appl. Bio. Mater. 2 (2019) 999–1005.
[138] W. Chen, J. Zhao, M. Hou, M. Yang, C. Yi, Nanoscale 13 (2021) 16197–16206.
[139] H. Song, Z. Cai, J. Li, H. Xiao, R. Qi, M. Zheng, J. Nanobiotechnology 20 (2022) 1–11.
[140] H. Zhang, S. Bo, K. Zeng, J. Wang, Y. Li, Z. Yang, X. Zhou, S. Chen, Z.-X. Jiang, J. Mater. Chem. B 8 (2020) 4469–4474.
[141] X. Liang, M. Chen, P. Bhattarai, S. Hameed, Y. Tang, Z. Dai, ACS Nano 15 (2021) 20164–20180.
[142] J. Li, D. Wei, Q. Fu, Nanoscale 15 (2023) 14790–14799.
[143] B.-R. Xie, Y. Yu, X.-H. Liu, J.-Y. Zeng, M.-Z. Zou, C.-X. Li, X. Zeng, X.-Z. Zhang, Biomaterials 272 (2021) 120782.
[144] Q. Chen, Z. Liu, Adv. Mater. 28 (2016) 10557–10566.
[145] G. Zhu, G.M. Lynn, O. Jacobson, K. Chen, Y. Liu, H. Zhang, Y. Ma, F. Zhang, R. Tian, Q. Ni, Nat. Commun. 8 (2017) 1954.
[146] X. Li, H. Fan, T. Guo, H. Bai, N. Kwon, K.H. Kim, S. Yu, Y. Cho, H. Kim, K.T. Nam, J. Yoon, X.-B. Zhang, W. Tan, ACS Nano 13 (2019) 6702–6710.
[147] X. Li, S. Yu, Y. Lee, T. Guo, N. Kwon, D. Lee, S.C. Yeom, Y. Cho, G. Kim, J.-D. Huang, J. Yoon, J. Am. Chem. Soc. 141 (2019) 1366–1372.

[148] X. Li, Y.-H. Jeon, N. Kwon, J.-G. Park, T. Guo, H.-R. Kim, J.-D. Huang, D.-S. Lee, J. Yoon, Biomaterials 266 (2021) 120430.
[149] X. Li, K. Jeong, Y. Lee, T. Guo, D. Lee, J. Park, N. Kwon, J.-H. Na, S.K. Hong, S.-S. Cha, J.-D. Huang, S. Choi, S. Kim, J. Yoon, Theranostics 9 (2019) 6412–6423.
[150] T. Zhao, Y. Xu, R. Liu, X. Shang, C. Huang, W. Dong, M. Long, B. Zou, X. Wang, G. Li, Adv. Healthc. Mater. 12 (2023) 2301035.
[151] X. Li, B.-Y. Zheng, M.-R. Ke, Y. Zhang, J.-D. Huang, J. Yoon, Theranostics 7 (2017) 2746–2756.
[152] X. Li, S. Yu, D. Lee, G. Kim, B. Lee, Y. Cho, B.-Y. Zheng, M.-R. Ke, J.-D. Huang, K. T. Nam, X. Chen, J. Yoon, ACS Nano 12 (2018) 681–688.
[153] K. Zheng, X. Liu, M. Li, S. Zhou, C. Ding, Anal. Chem. 94 (2022) 15067–15075.
[154] A. Ouyang, D. Zhao, X. Wang, W. Zhang, T. Jiang, A. Li, W. Liu, J. Mater. Chem. B 10 (2022) 306–320.
[155] Z. Wang, T. Jia, Q. Sun, Y. Kuang, B. Liu, M. Xu, H. Zhu, F. He, S. Gai, P. Yang, Biomaterials 228 (2020) 119569.
[156] S. Li, L. Zhao, R. Chang, R. Xing, X. Yan, Chem. Eur. J. 25 (2019) 13429–13435.
[157] J. Zhao, K. Xu, W. Yang, Z. Wang, F. Zhong, Chem. Soc. Rev. 44 (2015) 8904–8939.
[158] V.-N. Nguyen, J. Ha, M. Cho, H. Li, K. Swamy, J. Yoon, Coord. Chem. Rev. 439 (2021) 213936.
[159] W. Zhang, A. Ahmed, H. Cong, S. Wang, Y. Shen, B. Yu, Dyes Pigm. 185 (2021) 108937.
[160] H. Lu, J. Mack, Y. Yang, Z. Shen, Chem. Soc. Rev. 43 (2014) 4778–4823.
[161] B. Li, X. Xie, Z. Chen, C. Zhan, F. Zeng, S. Wu, Adv. Funct. Mater. 28 (2018) 1800692.
[162] M. Li, Y. Xu, Z. Pu, T. Xiong, H. Huang, S. Long, S. Son, L. Yu, N. Singh, Y. Tong, Proc. Natl. Acad. Sci. U.S.A. 119 (2022) e2210504119.
[163] M. Li, R. Tian, J. Fan, J. Du, S. Long, X. Peng, Dyes Pigm. 147 (2017) 99–105.
[164] M. Li, S. Long, Y. Kang, L. Guo, J. Wang, J. Fan, J. Du, X. Peng, J. Am. Chem. Soc. 140 (2018) 15820–15826.
[165] F. Xue, P. Wei, X. Ge, Y. Zhong, C. Cao, D. Yu, T. Yi, Dyes Pigm. 156 (2018) 285–290.
[166] C.T. Supuran, Nat. Rev. Drug Discov. 7 (2008) 168–181.
[167] H.S. Jung, J. Han, H. Shi, S. Koo, H. Singh, H.-J. Kim, J.L. Sessler, J.Y. Lee, J.-H. Kim, J.S. Kim, J. Am. Chem. Soc. 139 (2017) 7595–7602.
[168] C. Shi, M. Li, Z. Zhang, Q. Yao, K. Shao, F. Xu, N. Xu, H. Li, J. Fan, W. Sun, Biomaterials 233 (2020) 119755.
[169] Y. Cakmak, S. Kolemen, S. Duman, Y. Dede, Y. Dolen, B. Kilic, Z. Kostereli, L. T. Yildirim, A.L. Dogan, D. Guc, Angew. Chem. Int. Ed. 50 (2011) (1941) 11937.
[170] R.L. Watley, S.G. Awuah, M. Bio, R. Cantu, H.B. Gobeze, V.N. Nesterov, S.K. Das, F. D'Souza, Y. You, Chem. Asian J. 10 (2015) 1335–1343.
[171] H. van Willigen, G. Jones, M.S. Farahat, J. Phys. Chem. 100 (1996) 3312–3316.
[172] P. Zhao, Z. Wang, Y. Wang, Z. Wu, Y. Guo, C. Wang, X. Fang, Z. Qu, H. Wang, G. Zhao, Dyes Pigm. 214 (2023) 111214.
[173] L. Wang, Y. Qian, Biomater. Sci. 11 (2023) 1459–1469.
[174] Q. Zhang, P. Yu, Y. Fan, C. Sun, H. He, X. Liu, L. Lu, M. Zhao, H. Zhang, F. Zhang, Angew. Chem. Int. Ed. 133 (2021) 4013–4019.
[175] K. Li, X. Duan, Z. Jiang, D. Ding, Y. Chen, G.-Q. Zhang, Z. Liu, Nat. Commun. 12 (2021) 2376.
[176] J. Li, X. Du, X. Zhou, J. Yoon, Adv. Healthc. Mater. 12 (2023) e2301022.
[177] D. Xi, M. Xiao, J. Cao, L. Zhao, N. Xu, S. Long, J. Fan, K. Shao, W. Sun, X. Yan, Adv. Mater. 32 (2020) 1907855.
[178] D.-C. Yang, L.-F. Wen, L. Du, C.-M. Luo, Z.-Y. Lu, J.-Y. Liu, Z. Lin, ACS Appl. Mater. Inter. 14 (2022) 40546–40558.
[179] J. Li, X. Lv, J. Li, W. Jin, Z. Chen, Y. Wen, Z. Pei, Y. Pei, Org. Chem. Front. 10 (2023) 1927–1935.
[180] H. Geng, W. Lin, J. Liu, Q. Pei, Z. Xie, J. Mater. Chem. B 11 (2023) 5586–5593.
[181] Y. Tang, L. Xue, Q. Yu, D. Chen, Z. Cheng, W. Wang, J. Shao, X. Dong, ACS Appl. Bio. Mater. 2 (2019) 5888–5897.
[182] Y. Liu, N. Song, Z. Li, L. Chen, Z. Xie, Dyes Pigm. 160 (2019) 71–78.
[183] M. Zhao, Q. Zeng, X. Li, D. Xing, T. Zhang, Nano Res. 15 (2022) 716–727.
[184] Y. Tian, H. Zhou, Q. Cheng, H. Dang, H. Qian, C. Teng, K. Xie, L. Yan, J. Mater. Chem. B 10 (2022) 707–716.
[185] M. Jiang, J. Zhang, Y. Li, T. Shi, T. Ma, Y. Sun, H. Qiu, Y. Li, S. Yin, Mater. Chem. Front. 7 (2023) 3668–3679.
[186] W. Huang, H. Yang, Z. Hu, Y. Fan, X. Guan, W. Feng, Z. Liu, Y. Sun, Adv. Healthc. Mater. 10 (2021) 2101003.
[187] W. Lin, W. Zhang, S. Liu, Z. Li, X. Hu, Z. Xie, C. Duan, G. Han, ACS Appl. Mater. Inter. 11 (2019) 43928–43935.
[188] J. Luo, Z. Xie, J.W. Lam, L. Cheng, H. Chen, C. Qiu, H.S. Kwok, X. Zhan, Y. Liu, D. Zhu, Chem. Comm. (2001) 1740–1741.
[189] J. Mei, N.L. Leung, R.T. Kwok, J.W. Lam, B.Z. Tang, Chem. Rev. 115 (2015) (1940) 11718.
[190] Y. Tu, J. Liu, H. Zhang, Q. Peng, J.W. Lam, B.Z. Tang, Angew. Chem. Int. Ed. 131 (2019) 15053–15056.
[191] C.-J. Zhang, Q. Hu, G. Feng, R. Zhang, Y. Yuan, X. Lu, B. Liu, Chem. Sci. 6 (2015) 4580–4586.
[192] Y. Yuan, C.-J. Zhang, S. Xu, B. Liu, Chem. Sci. 7 (2016) 1862–1866.
[193] C. Zhang, Y. Zhao, D. Li, J. Liu, H. Han, D. He, X. Tian, S. Li, J. Wu, Y. Tian, Chem. Comm. 55 (2019) 1450–1453.
[194] F. Hu, S. Xu, B. Liu, Adv. Mater. 30 (2018) 1801350.
[195] Y. Hu, S.Y. Yin, W. Liu, Z. Li, Y. Chen, J. Li, Aggregate 4 (2023) e256.
[196] H. Zhao, N. Li, C. Ma, Z. Wei, Q. Zeng, K. Zhang, N. Zhao, B.Z. Tang, Chin. Chem. Lett. 34 (2023) 107699.
[197] Y. Li, R. Tang, X. Liu, J. Gong, Z. Zhao, Z. Sheng, J. Zhang, X. Li, G. Niu, R. T. Kwok, ACS Nano 14 (2020) 16840–16853.
[198] A.L. Antaris, H. Chen, K. Cheng, Y. Sun, G. Hong, C. Qu, S. Diao, Z. Deng, X. Hu, B. Zhang, Nat. Mater. 15 (2016) 235–242.
[199] H. Zhou, X. Zeng, A. Li, W. Zhou, L. Tang, W. Hu, Q. Fan, X. Meng, H. Deng, L. Duan, Nat. Commun. 11 (2020) 6183.
[200] K. Wen, H. Tan, Q. Peng, H. Chen, H. Ma, L. Wang, A. Peng, Q. Shi, X. Cai, H. Huang, Adv. Mater. 34 (2022) 2108146.
[201] X. He, Y. Luo, Y. Li, Y. Pan, R.T. Kwok, L. He, X. Duan, P. Zhang, A. Wu, B.Z. Tang, J. Li, Aggregate 5 (2023) e396.
[202] J. Zhuang, B. Wang, H. Chen, K. Zhang, N. Li, N. Zhao, B.Z. Tang, ACS Nano 17 (2023) 9110–9125.
[203] Y. Wang, S. Xu, L. Shi, C. Teh, G. Qi, B. Liu, Angew. Chem. Int. Ed. 60 (2021) 14945–14953.
[204] D. Zhao, H.-H. Han, L. Zhu, F.-Z. Xu, X.-Y. Ma, J. Li, T.D. James, Y. Zang, X.-P. He, C. Wang, ACS Appl. Mater. Inter. 4 (2021) 7016–7024.
[205] M.-Y. Wu, Z.-J. Wu, Q. Zou, J.-L. Wang, C. Kam, S. Chen, S. Feng, Chem. Eng. J. 454 (2023) 140189.
[206] Y. Xiao, Y. Yuan, M. Liang, J. Ni, L. Yu, Z.-S. Huang, B. Du, Y.-Y. Quan, Dyes Pigm. 220 (2023) 111765.
[207] L. Pan, S. Wang, M. Xie, M. Liang, L. Yu, B. Du, X. Ye, Y. Luo, Y.-Y. Quan, Z.-S. Huang, Mater. Des. 235 (2023) 112441.
[208] Y. Zhao, K. Xue, J. Deng, Z. Qi, Sens. Actuators B Chem. 393 (2023) 134255.
[209] Y. Wang, C. Zhang, Y. Li, R. Li, J. Li, L. Feng, Dyes Pigm. 218 (2023) 111517.
[210] S. Wang, Y. Liao, Z. Wu, Y. Peng, Y. Liu, Y. Chen, L. Shao, Z. Zeng, Y. Liu, Materials Today Bio 21 (2023) 100721.
[211] D. Wang, H. Su, R.T. Kwok, X. Hu, H. Zou, Q. Luo, M.M. Lee, W. Xu, J.W. Lam, B. Z. Tang, Chem. Sci. 9 (2018) 3685–3693.
[212] S. Martin, R.G. Parton, Nat. Rev. Mol. Cell Biol. 7 (2006) 373–378.
[213] K. Hasrat, X. Wang, Y. Li, L. Yang, Y. Zhao, K. Xue, X. Wang, J. Deng, J. Liang, Z. Qi, Dyes Pigm. 211 (2023) 111096.
[214] X. Li, W. Xu, Z. Yang, S. Li, X. Gu, T. Yuan, C. Li, Y. Wang, J. Hua, Sens. Actuators B Chem. 375 (2023) 132892.
[215] H. Shen, Y. Li, X. Kang, J. Wu, R. Chen, X. Wei, X. Zhang, J. Qi, Q. Liu, ACS Appl. Nano Mater. 6 (2023) 6056–6065.
[216] Y. Dai, H. Li, Y. Fu, J. Zhang, X. Zhang, Dyes Pigm. 220 (2023) 111782.
[217] Z. Zheng, T. Zhang, H. Liu, Y. Chen, R.T. Kwok, C. Ma, P. Zhang, H.H. Sung, I. D. Williams, J.W. Lam, ACS Nano 12 (2018) 8145–8159.
[218] H. Ma, C. Zhao, H. Meng, R. Li, L. Mao, D. Hu, M. Tian, J. Yuan, Y. Wei, ACS Appl. Mater. Inter. 13 (2021) 7987–7996.
[219] S. Li, X. Jin, Z. Zhang, J. Li, J. Hua, Mater. Chem. Front. 7 (2023) 3738–3746.
[220] H. Hu, D. Li, W. Dai, Q. Jin, D. Wang, J. Ji, B.Z. Tang, Z. Tang, Adv. Funct. Mater. (2023) 2213134.
[221] L. Yuan, Y. Su, B. Yu, Y. Shen, H. Cong, Biomater. Sci. 11 (2023) 985–997.
[222] J. Cui, F. Zhang, D. Yan, T. Han, L. Wang, D. Wang, B.Z. Tang, Adv. Mater. 35 (2023) 2302639.
[223] H. Shen, B. Wu, Q. Zhang, J. Ni, M. Liang, Y. Liu, X.-F. Zang, S. Wang, Y.-Y. Quan, X. Ye, Z.-S. Huang, Chem. Eng. J. 468 (2023) 143726.
[224] L. Lei, F. Yang, X. Meng, L. Xu, P. Liang, Y. Ma, Z. Dong, Y. Wang, X.-B. Zhang, G. Song, J. Am. Chem. Soc. 145 (2023) 24386–24400.
[225] Y. Liu, L. Teng, X.-F. Lou, X.-B. Zhang, G. Song, J. Am. Chem. Soc. 145 (2023) 5134–5144.
[226] Y. Liu, L. Teng, B. Yin, H. Meng, X. Yin, S. Huan, G. Song, X.-B. Zhang, Chem. Rev. 122 (2022) 6850–6918.
[227] Y. Ma, W. Sun, Z. Ye, L. Liu, M. Li, J. Shang, X. Xu, H. Cao, L. Xu, Y. Liu, Sci. Adv. 9 (2023) eadh1037.
[228] Y. Ma, J. Shang, L. Liu, M. Li, X. Xu, H. Cao, L. Xu, W. Sun, G. Song, X.-B. Zhang, J. Am. Chem. Soc. 145 (2023) 17881–17891.